Molecular Dynamics Determination of Two-dimensional Nucleation Kinetic Coefficient for Modeling the Faceted Growth of Si (111) from an Undercooled Melt

Victor Fabiyi[a], Tyler Richmond[a], Brian T. Helenbrook[b], and Eunsu Paek[a,*]

a *Department of Chemical and Biomolecular Engineering, Clarkson University, 8 Clarkson Avenue, Potsdam, NY 13699, USA*

b *Department of Mechanical and Aeronautical Engineering, Clarkson University, 8 Clarkson Avenue, Potsdam, NY 13699, USA*

Abstract

The discrepancies between kinetic model predictions and experimental observations of two-dimensional (2D) nucleation-mediated growth of silicon limits modeling reliability for existing and new crystal growth processes. Molecular dynamics (MD) simulations were performed to identify the mechanism of evolution of crystallites on a Si (111) facet and semi-quantitatively describe 2D nucleation kinetics using the forced-velocity solidification (FVS) and free-solidification (FS) MD simulations techniques. Both MD models predicted similar nucleation expressions but gave lesser nucleation energy barriers than predicted from Monte Carlo (MC) nucleation model. The estimated nucleation rate from MD was fitted to a polynuclear growth model to estimate a 2D kinetic model and compared to available experimentally reported growth rates. The Si (111) facet velocity model derived from the kinetic coefficient given in this work generally provided more conservative estimates of undercooling and the minimum undercooling that may result in kinetic roughening transition. In addition, the FVS model implemented in this work provided a unique opportunity for qualitatively describing the behavior of a crystal-melt interface and gave a molecular-level perspective on the interface stability criterion for the growth of single-crystal silicon during the horizontal ribbon growth (HRG) process.

Keywords: A1. Computer simulation, A1. Growth models, A2. Growth from melt, A2. Single crystal growth, B2. Semiconducting silicon, B3. Solar cells

*Corresponding author email address: *epaek@clarkson.edu* (Eunsu Paek)

1. Introduction

Two-dimensional (2D) nucleation is a critical process for the growth of crystals such as silicon that develop facets as they grow from the melt. During nucleation-controlled growth on a substrate, crystal layers are born on the faceted surface of the substrate and spread to fill the surface. Over the years, extensive investigations of Czochralski growth (CZ) [1]–[3] have revealed that undercooling is needed for new layers (i.e., facets) to nucleate during crystal growth. Upon nucleation of facets at the coolest part of the solid-liquid interface, they are propagated along steps vicinal to the crystal-melt interface before kinetic roughening sets in at higher undercooling. The faceting at the solid-liquid interface of silicon has received renewed research interest [4]–[6] in the development of the horizontal ribbon growth (HRG) [7]–[9] process for efficiently growing high-quality silicon crystals from undercooled melt for solar cell applications.

During the HRG process, low-defect crystals are grown by continuously pulling a thin sheet of crystalized material off from a pool of molten silicon, where the growth of the sheet is maintained by a cooling source such as a helium jet. The advantages of HRG over Czochralski growth include an extended surface area for efficient heat removal and latent heat dissipation, faster growth rates, minimal material losses [10], and cheaper wafer production cost [11]. Helenbrook *et al*. [4] recently identified the existence of a facet at the triple junction point (i.e., where solid liquid and gas meet), indicating that the growth edge should be modeled as a facet rather than a low-angle wedge [4], [5].

To better understand the behavior of the growth tip of HRG-silicon and predict growth limiting factors, knowledge of facet nucleation parameters is required. Much of our understanding of nucleation at solid-liquid interface comes from classical nucleation theory (CNT) [12]–[14]. According to CNT, the two-dimensional nucleation rate ( ), expressed as nucleation events per unit time and area, is an exponential function of the inverse of undercooling (Δ) represented as,

$$= \frac{1}{} = \exp\left(-\frac{}{}\right) = \exp\left(-\frac{^2}{_2\ \Delta}\right) \text{with} \quad = \frac{^2 T}{_2\ \Delta}, \qquad (1)$$

where $\frac{1}{}$ is the nucleation frequency of monolayer two-dimension islands, is the pre-exponential factor, is the Boltzmann constant, Δ is the undercooling, is the interfacial area, $_2$ is the mass per unit area of a single Si (111) layer of atoms, is the latent heat of fusion per unit mass,

and is the line tension between a layer of solid and liquid, is the nucleation energy barrier can, and T is the temperature.

Despite the availability of the CNT model, experimental investigation of nucleation is difficult, and the determination of physical parameters is uncertain [15]. For instance, determining the nucleation rate ( ) and line tension ( ) between the solid and liquid (described in **Eq. 1**) is complicated, and there are no verified data from the literature [16], [17]. The associated difficulty with nucleation and crystal growth experiments leaves the subject of determining parameters to computer simulations [18]–[26] because of their ability to model atomic interactions and describe the trajectory of atoms during phase change. Although simulations capture the fundamentals of realistic nucleation theories, they use relatively small ensembles accessible to the current computing power and idealized interatomic potential, allowing only qualitative comparisons with experiments [15]. However, simulation data may be fitted to a model [27] that considers the relative contribution of nucleation rates and step-growth velocity to provide some quantitative comparison with experimental data [18], [28].

The two computational tools commonly used for tracking the time evolution RIDWRPLFWHPSRUDO configuration are molecular dynamics (MD) and Monte Carlo (MC) simulations [15]. Although both models describe nucleation to be a stochastic process, MD models the phase space trajectory of an ensemble by solving NewWRQLDQ HTXDWLRQV RI PRWLRQ ZKLOH MC studies phase transitions in lattice models such as the Ising model [15], where a small change in free energy drives the change in thermodynamic properties. However, the time-dependent nature of nucleation from molecular simulations makes the attainment of steady-state nucleation rates more unlikely, with the departure from steady-state more pronounced for higher cooling rates (~500 K/ns) for a Lennard Jones liquid [15]. For instance, during quenching (cooling a liquid at high rates) simulations, unsteady nucleation arises from the fast-changing nature of cluster sizes before relaxation at a given temperature [15]. More recently, Prado *et al.* [29] employed MD to study the spontaneous nucleation of BaS from supercooled liquid and calculated steady-state nucleation rates that are valid for nucleation times larger than the typical relaxation time of supercooled liquids.

Despite the successes of MD in studying fundamental growth processes, to the best of our knowledge, MD has not been employed to quantitatively describe two-dimensional (2D) nucleation kinetics for the faceted growth of silicon on a silicon substrate. The silicon 2D kinetic

coefficient primarily used in analytical and numerical [4], [6], [30] modeling of faceted growth of silicon was derived from nucleation rate determined from MC simulations fitted to a growth model [27] to match experimentally observed growth rates [18]. However, the 2D kinetic coefficient presented in ref. [18] and its subsequently corrected version [31], [32] estimates critical undercooling as ~4.7 K, which differs by about 3.2 K compared to experimental observations [33] [37], and does not capture kinetic transitions within the undercooling regime experimentally reported [38], [39] for the growth of faceted dendrites. In this paper, we attempt to approximate a 2D nucleation rate model from molecular dynamics to provide an alternative kinetic model for describing the faceted growth behavior of silicon and possibly predict kinetic transition that may occur at elevated undercooling.

In this study, we implement two distinct MD solidification techniques, namely the free-solidification [19], [25], [26], [40] and the forced-velocity solidification (FVS) [21], [22], [41] models to assess reliability of molecular-level nucleation data. Our goal is to observe facet nucleation and growth, determine critical nucleation parameters for kinetic modeling, and discuss the fundamental behavior of an HRG crystal-melt interface. In the next section, we provide a comprehensive description of our computational methods followed by the discussion of results, including the evolution of crystallites on Si (111) via a 2D nucleation-controlled mechanism, the determination of 2D nucleation rates, determination of 2D kinetic model for prediction of undercooling, and the applicability of the FVS simulation model for the description of interface mobility and heat flow across the solid-liquid interface during HRG.

2. Interatomic Potential and Computational Method

In this work, MD simulations are performed using the large-scale atomic/molecularly massive parallel simulator (LAMMPS) [42]. We modeled the Si-Si interaction with the Stillinger-Weber (SW) potential [43], which is given by

$$( ) = \sum_{, (<)} {}_2(,) + \sum_{, , (< <)} {}_3(, ,) \qquad (3)$$

$${}_2( ) = \begin{cases} (\quad ^{-} - \quad ^{-}) \quad [\frac{}{-}] , & < \\ 0 & \geq \end{cases} \qquad (4)$$

111 $$\Phi_3(r_{ij}, r_{ik}, \theta_{ijk}) = \left[\lambda \exp\left(\frac{\gamma}{r_{ij}-a} + \frac{\gamma}{r_{ik}-a}\right)\right]\left[\cos\theta_{ijk} - \cos\theta_0\right]^2 \quad (5)$$

112 The SW potential describes the interactions between silicon atoms *i* and *j* as a sum of two-body
113 and three-body interactions. The 2-body potential energy term Φ_2 in **Eq. 4** is a function of radial
114 distance r_{ij} between the interacting atoms and is defined as a combination of exponential and
115 inverse power functions. In **Eq. 4**, A is a constant in energy units, σ is a constant in distance units,
116 while B, p, q, and a are all unitless constants. On the other hand, **Eq. 5** gives the 3-body potential
117 energy term (Φ_3) as a function of three-way radial distances r_{ij} and r_{ik} between three interacting
118 silicon atoms. Here, λ and γ are unitless constants, θ_{ijk} is the angle between r_{ij} and r_{ik}, and θ_0
119 is a constant equal to -1/3. **Eq. 5** combines exponential and cosine functions that account for the
120 translational and rotational symmetry of the diamond structure of crystalline silicon.

121 FVS simulations involve applying a uniform displacement to all atoms every timestep in a
122 direction perpendicular to a crystal-melt interface located between two heat baths. This establishes
123 a macroscopically steady growth scenario. The interface temperature is then monitored as a
124 function of steady-state growth rate to investigate kinetics. Conversely, in the FS simulations, a
125 uniform temperature below melting point is applied to a crystal-melt simulation domain such that
126 crystals grow into the undercooled melt at a rate comparable to the expansion of the solid domain.
127 For both simulation techniques, the following initialization procedure was used to generate the
128 solid-liquid cell. We set up a simulation cell containing 36,864 crystal atoms with dimensions
129 46.33 × 53.50 × 300.69 $Å^3$. The interfacial area employed here is considered large enough to
130 avoid finite-size effects based on previous works [19], [22]. We used a lattice spacing of 5.43 Å,
131 oriented silicon (111) along the z-axis to serve as the growth direction and applied periodic
132 boundary conditions in all axes. Next, the system's potential energy was minimized, and random
133 Gaussian velocities were assigned to all atoms, followed by equilibration at 1000 K for 50 ps. The
134 system was placed in a canonical ensemble while heated to a temperature of 1525 K□ a value
135 lower than the reported equilibrium temperature range (i.e., 1677-1692 K) [19], [44]□[46] for SW
136 silicon□ and equilibrated for 100 ps. Half of the cell was melted by heating to 3000 K and
137 equilibrating for 100 ps, keeping the crystal half fixed. The melt region is then cooled to a
138 temperature of 2125 K, a temperature significantly higher than SW silicon melting point, and then

equilibrated for 100 ps. The resulting solid-liquid configuration (see **Fig. 1**) served as the starting point for the production runs for both the FVS and FS simulations.

In crystal growth simulations from initial solid-liquid cells, the size of solid and liquid domains may be even [19], [22], or a larger liquid domain [21] may be used to minimize artifacts. Since FVS has not been implemented for SW silicon, we conducted initial simulations (summarized in **Fig. S1-2** of the **supporting information**) to determine the appropriate solid-liquid configuration. Our findings showed that a configuration with a larger liquid domain and a small thermal gradient (~0.36 K/Å) applied across the heat source and sink allowed for a narrow pull speed range (0.01 - 0.02 Å/ps) that kept the interface far from the heat sink, resulting in insufficient data for establishing growth-undercooling relationships. Hence, we implemented a simulation domain (**Fig. 1a**) with a large thermal gradient of ~4.63 K/Å applied across the solidification and melting fronts. The temperature was maintained at 1525 K and 2125 K within two evenly-spaced thin regions (of thickness ~17 Å) by velocity rescaling using the Berendsen thermostat [47] relaxed every 0.1 ps. Next, continuous pulling at velocities (v) ranging from 0 - 0.045 Å/ps was imposed on the entire system by adding vdt displacements to all atoms every time step (dt) in the growth direction. Desired pulling speed is reassigned every nanosecond to minimize drifting since the system's momentum is not fixed. For energy conservation, the entire domain was placed in a microcanonical ensemble (NVE) so that the number of atoms (N), the volume (V), and energy (E) stayed constant throughout the simulation. Thermodynamic properties are monitored with simulation time until the macroscopic properties reached steady-state and the interface became immobile.

In the FS simulations shown in **Fig. 1b**, solidification was carried out in canonical ensemble (NPT) with a constant number of atoms (N), pressure (P), and temperature (T). We fixed the x and y dimensions of the cell, controlled only the z-component of pressure ($P_z = 0$) using the Nose-Hoover algorithm, and varied the solidification temperature (i.e., thermostat set temperature) between 1647 and 1674 K. The growth rate in the z-direction, is estimated using

$$= \frac{3}{2} \cdot \text{—}, \qquad (6)$$

where is lattice spacing equal to 5.43 Å, is the number of atoms in diamond silicon crystal structure equal to 8, is the area of the interface, and —— is the liquid-to-solid conversion rate of silicon atoms.

For all simulations, the integration of Newton's equation of motion was performed using the velocity Verlet algorithm [48] at a timestep of 1 fs. Simulations at a given pulling speed for the FVS model or temperature for the FS model were independently reproduced over three initial solid-liquid configurations to ensure statistical accuracy.

3. Results and discussion

3.1. Observation of Crystal Growth

This section explains the nucleation and growth behaviors of the forced-velocity solidification (FVS) and free-solidification (FS) molecular dynamics (MD) models. The extended version of the common neighbor analysis (CNA) implemented by Maras *et al.* [49], [50] in the Open Visual Tool (OVITO) [51] program is used to distinguish liquid and crystalline structures because of its suitability for materials that crystallize in the diamond structures like silicon [52]. **Figure 2** shows the molecular-level crystal growth process from solid-liquid interfaces, with the snapshot at 0 ns representing the initial solid-liquid configuration before the onset of crystallization. The atomic arrangements of atoms corresponding to the different color codes given in **Fig. 2** are presented in **Fig S3** to show the single-crystal atoms are grown on each monolayer. For the FVS model, solidification□ and melting□ is continuous after reaching a steady-state (at ~4 ns as shown in **Fig. S4a**) irrespective of the pulling speed imposed on the system. For example, at a pulling rate of 0.02 Å/ps, the red-colored reference crystal layer (i.e., lower red-colored at 0 ns) in **Fig. 2a** is pulled across an axial distance equivalent to ~48 layers thickness (a single layer thickness is 3.13 Å) before melting after ~8.5 ns of constant pulling, yielding approximate growth/melting rates of 0.018 Å/ps. In general, the measured growth rate from the FVS technique was found to be 13% lower than the requested pull speed (plotted in **Fig. S4b)**, which we corrected by using the measured growth rate for all calculations.

On the other hand, in the FS model shown in **Fig. 2b**, ~ 18 layers nucleate and grow from each of the two initial solid-liquid interfaces (i.e., the layers with light blue atoms at 0 ns) as the

undercooled silicon melt is consumed (diminishing of the grey liquid particles), highlighting the transient nature of the solidification front. One of the difficulties with the FS model is tracking the interface temperature and position because of the movement of the growth interfaces until the entire simulation domain is crystallized, so the thermostat temperature is generally taken as the interface temperature.

3.2. Atomic Evolution of Crystallite

In **Fig. 2**, the crystal-melt interfaces remained atomically flat for relatively large undercooling and growth rates. The observation of flat interfaces is not surprising from MD simulations as Buta *et al.* [19] reported silicon solid-liquid interfaces at undercooling up to 40 K. Fujiwara [53] attributed the molecular-scale planar interface to high step velocities measured on the Si (111) interfaces. In this section, by back-tracking the trajectory of a monolayer-thick slice to observe the changes in the atomic arrangement of atoms inside the slice as they approach the interface from the melt phase, we discuss the origins of the planar interface seen in MD for Si (111) facet and fundamentally explain the mechanism of 2D nucleation. An example from the FVS simulation at a pulling speed of ~0.01 Å/ps is presented in **Fig. 3a.** The inset figures show the crystal coverage of the interface with liquid atoms removed for a more precise observation of the process. From **Fig. 3a**, ~ 50 crystal atoms (crystallites) emerge from the melt at a distance of ~3.13Å, equivalent to one layer thickness away from the stationary interface. However, crystallites growth was slow until an interface coverage of 0.4 was reached due to the competition between the formation and dissolution of crystallites. Interestingly, the surface coverage of 0.4 corresponds to a cluster size of ~ 150 atoms, consistent with the approximate critical cluster size required for the growth of silicon crystallites [23], [24]. As the slice moved closer to the interface, the clusters grew more rapidly, and their atomic arrangement became more orderly. Other samples layers (not shown here) from both MD models showed a similar crystallite growth trend.

Also, in **Fig. 3b**, we illustrate the mechanism for continuous growth in the FVS domain by considering the trajectory of a single layer (upper panels) sitting atop a flat one-layer thick Si (111) substrate (bottom panels) that had earlier evolved from the melt phase. The circles in the upper panel at 30 ps show nucleation sites inside a pool of undercooled melt. As simulation time proceeded to 90 ps, smaller adjacent clusters grew and merged to form an oversized island that expanded to create a nearly complete layer at 200 ps. The corresponding snapshots of the substrate

layer shown in the bottom panels show that a substrate layer is almost entirely formed (~ 90%) before another 2D island nucleates above it, indicating that growth occurs layer-by-layer. The molecular observation presented here sheds some light on the competing mechanisms of island nucleation and expansion. Typically, the island nucleation rate is predicted to be either faster than the island expansion rate or vice versa [12] [25]. In the former scenario, nucleation time is short so that more than one nucleus□ and consequently more than one layer□ may grow simultaneously (polynuclear growth). By contrast, for a faster island expansion rate, a nucleus formed in a pool of undercooled melt spreads in a two-dimensional manner to form a single layer which becomes a substrate for the next layer to grow, and so on. However, the observations from this work suggest that both events may not be entirely mutually exclusive on an atomic level. The rapid island expansion underlying the layer-by-layer growth mode from MD simulations results from the nucleation and merger of smaller crystallites atop the substrate layer to form a critical-sized single bi-dimensional island that eventually fills the surface. Hence, we provide an atomic-level understanding of the origins of flat crystal-melt interfaces during the nucleation-mediated growth of crystals from undercooled melt.

3.3. Nucleation Rate-undercooling Relationship

The relationship between solidification rate and undercooling (7□) is derived from the MD simulation. The undercooling is estimated as the difference between interface temperature (T) and the equilibrium melting temperature. Here, equilibrium melting temperature corresponds to the interface temperature (~1691 K) at roughly zero-growth velocity for the FVS simulations and a temperature of ~1677 K [19] for the FS simulations. In the FVS simulation, the measured growth rates are known from the pulling speeds ranging from 0.01□0.045 Å/ps, so their corresponding interface temperatures are determined from the intersections of the fitted thermal profile of the solid and liquid domains that developed inside the solidification front, as illustrated in **Fig. 4a** for a growth rate of ~0.01 Å/ps. On the other hand, the addition of one Si (111) layer thickness (corresponding to 384 interfacial atoms) at a time for a temperature range of 1647 □1671 K (shown in **Fig. 4b**) in the FS simulation domain indicate layer by layer growth until the domain if fully crystallized. The T = 1671 and 1665 K curves show nucleation-limited growth with long pauses between nucleation and layer growth, but the average time for monolayer nucleation becomes shorter as the undercooling increases. The trend in layer addition in the FS model is qualitatively

similar to that of ref. [18] but a quantitative comparison of the MD and MC predictions may be difficult due to differences in the time and length scales. For instance, at equal undercooling of 18

The best-fit slopes from **Fig. 4b** are inserted to **Eq. 6** to determine the axial growth rates at the respective growth temperatures (or undercooling).

Assuming the time between the nucleation of each Si (111) monolayer represents the average time between critical nucleation events, the average two-dimensional nucleation rate can be estimated at each undercooling since the interfacial area is known. For the nucleation rates, (in units of $m^{-2}s^{-1}$), plotted in **Fig. 4c**, we focused on moderate undercooling that gave the linear responses between the logarithm of nucleation rates and reciprocals of undercooling ($1/\Delta$). For FVS and FS simulations, undercooling values greater than 24 K and 12 K were respectively considered. Expressions similar to **Eq. 1** were derived from data shown in **Fig. 4c** to extract the pre-exponential and exponential factors. The individual nucleation rate models derived for the FVS and FS models are $10.0\times10^{7}exp(-\frac{4590}{\Delta})$ and $64.0\times10^{6}exp(-\frac{3833}{\Delta})$, respectively as shown in see **Fig. S5a**. The contrast between the MD methods suggests nucleation rates may be slightly faster in the FVS model within a higher undercooling regime, and rates in the FS model may proceed more quickly as the undercooling approaches zero. The slight disparity between predictions of both MD methods may be related to the precision of interface temperature. For the FVS, interface temperature is determined at the solid-liquid junction, accounting for latent heat release during phase change which is not the case for FS simulations where a thermostat controls the interface temperature [54]. The latent heat release is expected to warm up the FVS interface, resulting in lesser undercooling for comparable growth rates and consequently larger nucleation kinetics than predicted by the FS model. However, from **Fig. 4c**, we see that the nucleation rates predicted by the FVS and FS models are pretty consistent in the overlapping undercooling region. Thus, a best-fit for the nucleation rate-undercooling relationship derived by combining the FVS and FS MD nucleation data shown in **Fig. 4c** is $_{2}(\quad) = 90.0\times10^{6}exp(-\frac{4391}{\Delta})$ The MD nucleation rate compares to $11.5\times10^{7}exp(-\frac{140}{\Delta})$ estimated from the MC method [18], [31] (also shown in **Fig. 4c)**. The MD and MC results comparison implies that the faster nucleation and growth rates observed in MD may be attributed to the lower (~ 69%) nucleation energy barrier required to form a Si (111) layer. However, nucleation rates from MD and MC model become comparable at

infinitely large undercooling as the pre-exponential factors differ by only ~ 8%. While the disparity between the MC and MD prediction of nucleation parameters may explain why crystal layers grow faster in the MD domain at comparable undercooling as observed in **Section 3.3,** the cause of the disparity is tricky to explain. It is uncertain how the MC time and length scale differs from our MD simulations since ref [18] did not explicitly describe their solidification configuration and simulation domain size. Alternatively, we may explain the lower nucleation barrier from MD simulations by the fact that the nucleation of the critical-sized 2D cluster from the merger of undersized clusters occurs atop a well-formed Si (111) crystal (substrate) layer [19].

3.4. Prediction of Undercooling for Experimentally Reported Facet Growth Rates

Although nucleation rates from computer simulations occur on time and length scales inaccessible by experiments, Obreten and co-worker [27] proposed a facet velocity, , model independent of surface area and valid for higher growth velocities. This model is given by:

$$= \quad \frac{1}{3}\ \frac{2}{3}\quad \frac{1}{3}\ , \qquad (7)$$

where is the height of a single layer (3.13 Å), is the two-dimensional nucleation rate, is the spreading velocity of a monolayer step, is a numerical coefficient near unity (~0.97), is a geometric factor (for circle and 4 for square). We take = 0.63 Δ m/s [30] which is consistent with MD [19] and experimental [55] predictions and MD approximation of nucleation rate for to estimate a 2D nucleation kinetic coefficient (in m/s/K units) given by $3.4 2\times 10^{1} exp(-\frac{1.464}{\Delta})\Delta^{-}$. This coefficient compares to $2.2 2\times 10^{1} exp(-\frac{4.667}{\Delta})\Delta^{-}$ estimated from MC data given in ref. [18].

Using parameters from molecular dynamics, the facet growth rate model in **Eq. 7** is extrapolated to low undercooling values not captured in the nucleation model determined from simulation data as shown in **Fig. 5.** Using the facet velocity versus undercooling curve (**Fig. 5**), the undercooling at experimentally reported solidification rates can be predicted. For comparison, the curve predicted from the MC simulation-derived 2D kinetic model is provided as well. Firstly, at a typical CZ growth rate of 3×10^{-5} m/s (see inset of **Fig. 5)**, the MD kinetic model gives an undercooling of 1.5 K compared to 4.7 K approximated from MC kinetic coefficient by Beatty and Jackson [18]. Although experimental validation of simulation prediction is tricky due to varying

conditions at which experiments were performed, reliable investigations for low-defect facet nucleation and growth estimated undercooling to be between 1.5 and 1.7 K for CZ growth rate [56], [57].

With increasing undercooling, there is an exponential surge in facet growth rate. We assume the surge in growth rate corresponds to kinetic roughening transition known to occur at higher undercooling [28]. Physically, kinetic transitioning indicates a change in growth mechanisms associated with the transformation of grown crystal structures from single-crystalline to faceted-dendrite at higher undercooling, as suggested by recent *in situ* observations showing faceted-dendrites growth of silicon sets in at ~10 K undercooling [38], [39]. To estimate the onset of kinetic roughening, we found a linear fit for the growth rate-undercooling curve (i.e., an extension of **Fig. 5** shown in **Fig. S5b**) corresponding to 0.085 m/s/K, a value comparable with the rough growth kinetic coefficients (in units of m/s/K) of ~0.12 for the (100) orientation [19] and ~0.12/ $\sqrt{2}$(0.085) expected for the (110) orientation [22], [40]. The agreement between the linear fit and rough growth kinetics supports the argument of a kinetic transition at large undercooling. On the other hand, the linear fit for the extended MC curve also shown in **Fig. S5b** at higher undercooling resulted in a slope of 0.028 m/s/K, which is significantly smaller than the rough growth kinetic coefficient. Hence, the kinetic transition point is predicted by finding the least undercooling where there is a significant deviation between the linear fits described above and their corresponding original curves. The respective kinetic transitioning undercooling values extracted from the MD- and MC-based models are ~9.5 K and ~19.5 K, corresponding to 5% and 95% deviations from reported experimental observation of 10 K. The analysis presented in this section reveals that the MD-derived 2D kine8tic coefficient captures a possible kinetic transition at higher undercooling.

Next, we compare the prediction of the MD kinetic model to the experimentally reported rates for the horizontal ribbon growth (HRG) of silicon from its melt to approximate undercooling at corresponding growth rates and verify the possible growth regime. At a growth rate of 7×10^{3} m/s reported by Kudo *et al*.'s [58], the respective undercooling predicted from the MD and MC kinetic data are 3.2 K and 9.4 K. Bates and Jewett's [59] growth rate of 14×10^{2} m/s corresponds to undercooling values of 3.6 K and 10.7 K from the MD and MC models, respectively. And lastly, at a growth rate of 2×10^{3} m/s reported by Helenbrook *et al*. [4], MD and MC kinetic models give undercooling values of 2.6 K and 7.7 K, respectively. For all the

experimental growth rates mentioned above, the MD-derived kinetic model gave lower estimates of undercooling than MC kinetic data. The disparity between the MD and MC facet velocity model predictions may be directly attributed to the differences in nucleation rates and step kinetics from both simulation techniques.

Interestingly, at reported HRG growth rates [4], [58], [59], the corresponding undercooling values estimated from the MD-derived kinetic model are below the experimental lower limit of 10 K for the kinetic transition. This observation suggests it may be possible to grow single crystals at growth rates (stated above), assuming faceted growth mechanism controls. However, the unexpectedly low limiting growth rates (2×10^{3} m/s) attained in the most recent HRG experiment [4] underscores the possibility of limiting factors such as heat flow, competing growth mechanisms in different crystallographic directions, grain boundary formation, or the presence of impurities in the melt. While we briefly discuss heat flow behavior across the crystal-melt interface here, the other limiting factors are subjects beyond the scope of this work and are currently being explored for future research.

3.5. Applicability of FVS to HRG

Lastly, we discuss the application of the FVS model for investigating the crystal-melt interface behavior of HRG-silicon. The constant-rate solidification at the solid-liquid interface located between a heat source and sink in the FVS approach closely models the HRG process in which molten silicon flows onto a cooled-flat surface for onward extraction of thin sheets of silicon at a constant pull speed. The cyclic melting and solidification in the FVS model are also akin to the melt replenishment that drives the continuous growth in horizontal growth processes. Although the FVS crystal-melt interface discussed here is considered a two-phase junction which is different from the HRG triple junction growth tip (i.e., comprising of a solid-liquid interface in contact with a gas phase), it provides a molecular perspective on the dynamics of heat flow within the bulk liquid and solid adjacent the interface.

The HRG is especially facilitated by the change in electrical and thermal properties of silicon as it goes through a liquid-solid phase change [60]. The potential energy and temperature profiles across the simulation cell with pull speed ranging from 0.005 to 0.045 Å/ps are presented in **Fig. 6**. The typical change in bulk properties (see **Fig. 6a**) from liquid to solid signifies phase change across an interface region approximately 12 Å wide. Beyond a pull speed of 0.04 Å/ps, increasing

uncertainty in interface position (i.e., the broadening of the interfacial width from the potential energy profile) within the solidification front develops, followed by the pulling of the interface against the heat sink (boundary of the solidification front) at higher growth rates. We focus on the pull speeds that kept the interface immobile within the solidification boundary for the discussion here.

During crystal growth from the melt, thermal gradients develop because of the evolution and absorption of latent heat [54]. Likewise, during phase transition in the FVS model, different temperature gradients evolve in the melt-side and crystal-side of the interface (see **Fig. 6b)** in response to the density drop (in a similar fashion as the potential energy drop shown in **Fig. 6a**) accompanying latent heat release. The linearity of the temperature profiles developed inside the solidification front stems from the large thermal gradient (4.63 K/Å) applied across the solidification front. As pulling speed increased, WKHPHOWVROLGLILFDWKHDWIOX[GHFUHDVHGIURPDWR 5.00 K/Å while WKHVROLGLILFDWLRQIURQWLQFUHDVHGIURPDWR in contrast, resulting in

$$\frac{-}{\qquad} - \frac{-}{\qquad} = \rho \quad , \qquad (9)$$

the downstream (leftward) movement of the crystal-melt interface observed in **Fig. 6a**. Similar trends were reported from both experiments and numerical simulations of the HRG process [4], [6], [11], [61]. We explain the physics of the shift in interface position by considering the crystal-melt interface boundary condition [60] for an established stable melt zone given by:

where constants , , , , ,and correspond to solid conductivity, liquid conductivity, the cold bath temperature, the hot bath temperature, solid density, and latent heat, respectively. Also, , and are interface temperature, lengths of solid, liquid domains, and pull speed, respectively. **Equation 9** considers only conductive heat transport in line with the previous prediction of dominant conductive heat flux during steady-state heat flow through the growth interface [6], [60]. The assumption of conductive heat flow dominating advection heat flow is reasonable for the FVS model considering the huge thermal gradient (the thermal gradient is proportional to the conductive heat flux) across the solidification front. Therefore, we expect the latent heat component (i.e., right side of **Eq. 9**) to increase with pulling speed. In response, the solid conductive heat flux (first term on the left side of **Eq. 9**) increases by shrinkage of the solid domain (decrease in) while the

liquid conductive heat flux decreases by expansion of liquid domain (increase in) to balance the increase in latent heat flux, leading to the downstream movement of the interface. Consequently, the solidification front boundary dictated by sets the limit for the pulling speed attainable for a given driving force (available solidification front thermal gradient).

The maximum pull speed from the FVS solidification model that maintained the interface within the solidification boundary was identified to be 0.04 Å/ps. Beyond this limiting pull speed, the crystal-melt interface became unstable due to the imbalance between the crystal contraction (~60% rise of thermal gradient estimated from **Fig. 6b**) and the melt expansion (~40% drop in thermal gradient calculated from **Fig. 6b**). The slower decline of the melt-side gradient compared to the rise of the crystal-side gradient implies a slow rate of heat removal from the melt, which is detrimental to the stability of the interface. For the first time using molecular-level simulations, we report that large heat flux in liquid is necessary for the stability of a growing ribbon at high pull speeds. Pirna and Helenbrook [6] reached a similar conclusion from analytical and numerical analyses that pull speed limitation during the HRG process depends on the magnitude of the heat flux in the liquid at the triple junction point (TJP). Noronha and Ydstie [62] also suggested the preferential heat removal from the liquid as a stability criterion for the TJP. In addition, this work offers a molecular dynamics perspective on the critical role of melt heat flux in the HRG process.

4. Conclusions

The main aim of this paper is to determine a two-dimensional kinetic coefficient from molecular dynamics (MD) that could describe the experimental growth rates of silicon single-crystals. Consequently, we employed forced-velocity solidification (FVS) and free solidification (FS) simulation techniques to model crystal-melt interfaces at different growth rates. In both MD methods, we report rapid nucleation and spreading of nuclei to form a complete layer atop a substrate followed by layer-by-layer growth of Si (111) layers. Notably, our extension of the FVS model to silicon provides a comprehensive account of an alternative molecular approach for studying nucleation and crystal growth processes. We show that the precision of interface position□ and by implication, interface temperature□ offered by the FVS method results in a significantly higher nucleation pre-exponential factor.

Furthermore, we determined the dependence of nucleation rates on undercooling from MD simulations and show that MD simulations predict lower activation energy barriers for the

nucleation of new silicon facets compared to MC simulation prediction. Consequently, the derived 2D kinetic coefficient (from MD nucleation data) extrapolated to lower undercooling values predicted relatively conservative undercooling values for experimentally observable growth rates reported from the CZ and HRG processes. Also, the MD-kinetic model captures the kinetic transition typically observed at higher growth rates and undercooling values. For practical applications, the kinetic model determined in this work could improve the modeling of silicon crystal growth processes compared to the currently available kinetic models.

Lastly, we provide a molecular-level analysis of steady-state heat flow across a crystal-melt interface of the FVS. The response of interface position to increased pull speed reported from atomistic simulations agreed with experimental and continuum-level observations for the horizontal ribbon growth of silicon from an undercooled melt. Furthermore, we report a pull speed limit related to heat transfer suggesting a substantial melt side heat flux is critical to stabilizing the crystal-melt interface at high pull speeds. The framework discussed in this work opens up an opportunity to study the dynamic behavior of crystal-melt interface during horizontal ribbon growth of silicon for different crystal orientations, which may improve our fundamental understanding of the origins of the relatively low HRG growth rates.

Acknowledgments

This work was supported by the National Science Foundation under grant CMMI-1762802. We

for use of their computing resources.

References

[1] J. R. Fiks, D. A. Vanlier, J. R. Zwikker, R. M. Lobel, and E. R. [illegible], *Journal of Crystal Growth*, vol. 65, no. 1–3, pp. 189–213, Dec. 1983, doi: 10.1016/0022-0248(83)90051-9.

[2] J. (J. R. P. van Hengel, D. J. R. Fikus, D. A. van Nieuwkoop, and [illegible] father of the J. R. Fikus, D. A. van Nieuwkoop, "HWR," *Journal of Crystal Growth*, vol. 236, no. 1, pp. 1–4, Mar. 2002, doi: 10.1016/S0022-0248(01)02195-9.

[3] [illegible]. H. Okrent, J. K. Hesse, M. L. F. van R. J. R. Fikus, D. A. van Nieuwkoop, J. R. Zwikker, and [illegible], *Nieuwkoperprobleme 27: Plenary Lectures of the Dorr Physiosnisc" "Semiconductors" "Fluids" "Dynamics" "Mechanics" "Megnetism" "Low Temperature Ph*

(DPG) Münster, M. Grosch, Ed. Berlin, Heidelberg: Springer, 1987, pp. 241–263. doi: 10.1007/BFb0107924.

[4] [illegible], *Journal of Crystal Growth*, vol. 453, pp. 163–172, Nov. 2016, doi: 10.1016/j.jcrysgro.2016.08.034.

[5] [illegible] Silicon Method single crystal ribbon [illegible] *Journal of Crystal Growth*, vol. 451, pp. 174–180, Oct. 2016, doi: 10.1016/j.jcrysgro.2016.07.012.

[6] [illegible] *Journal of Crystal Growth*, vol. 555, p. 125958, Feb. 2021, doi: 10.1016/j.jcrysgro.2020.125958.

[7] S. Williams, [illegible] Mar. 26, 2021. [Online]. Available: https://patents.google.com/patent/US3031275A/en

[8] [illegible] *Journal of Crystal Growth*, vol. 79, no. 1–3, pp. 572–577, Dec. 1986, doi: 10.1016/0022-0248(86)90522-1.

[9] [illegible] A new approach to high speed growth of silicon [illegible] *Journal of Crystal Growth*, vol. 104, no. 1, pp. 108–112, Jul. 1990, doi: 10.1016/0022-0248(90)90317-E.

[10] [illegible] Massachusetts Institute of Technology, 2011.

[11] [illegible] *Ind. Eng. Chem. Res.*, vol. 52, no. 9, pp. 3239–3246, Mar. 2013, doi: 10.1021/ie301857p.

[12] J. G. Dash, V. A. Hodgkin, and [illegible] *Journal of Statistical Physics*, vol. 95, no. 5, pp. 1311–1322, Jun. 1999, doi: 10.1023/A:1004579223189.

[13] [illegible] *Metallurgica*, vol. 8, no. 8, pp. 554–562, Aug. 1960, doi: 10.1016/0001-6160(60)90110-3.

[14] J. W. Cahn, "The Kinetics of Grain Boundary Nucleated Reactions," *Acta Metallurgica*, vol. 12, no. 12, pp. 1421–1439, Dec. 1964, doi: 10.1016/0001-6160(64)90130-0.

[15] J. J. Hoyt, "Atomistic Crystal Growth Theory," in *Pergamon Materials Series*, vol. 15, K. F. Kelton and A. L. Greer, Eds. Pergamon, 2010, pp. 363–389. doi: 10.1016/S1470-1804(09)01510-7.

[16] L. Zou, J. Wang, "Capillary wetting and dewetting of crystal multilayers at the air-water interface," *Phys. Rev. E*, vol. 76, no. 3, p. 031602, Sep. 2007, doi: 10.1103/PhysRevE.76.031602.

[17] J. J. Hoyt, "Calculation of the line tension in three-phase (solid-liquid-vapor) equilibrium," *Colloids and Surfaces A: Physicochemical and Engineering Aspects*, vol. 116, no. 1, pp. 43–54, Sep. 1996, doi: 10.1016/0927-7757(96)03651-5.

[18] J. J. Hoyt, "Capillary Anisotropy and Morphological Stability," *Journal of Crystal Growth*, vol. 211, no. 1, pp. 13–17, Apr. 2000, doi: 10.1016/S0022-0248(99)00836-2.

[19] J. J. Hoyt, "Capillary Anisotropy and Morphological Stability," *J. Chem. Phys.*, vol. 127, no. 7, p. 074703, Aug. 2007, doi: 10.1063/1.2754682.

[20] J. J. Hoyt, "Capillary Anisotropy and Morphological Stability," *Phys. Rev. E*, vol. 78, no. 3, p. 031605, Sep. 2008, doi: 10.1103/PhysRevE.78.031605.

[21] F. Celestini and J.-M. Debierre, "Line tension and the fluctuation regime of contact lines," *Phys. Rev. B*, vol. 62, no. 21, pp. 14006–14011, Dec. 2000, doi: 10.1103/PhysRevB.62.14006.

[22] F. Celestini and J.-M. Debierre, "Determination of the line tension of a solid-liquid-vapor system," *Phys. Rev. E*, vol. 65, no. 4, p. 041605, Apr. 2002, doi: 10.1103/PhysRevE.65.041605.

[23] D. M. Kolb, G. E. Engelmann, and J. C. Ziegler, "Anomalous Debye Screening in Concentrated Aqueous Electrolytes," *Phys. Rev. B*, vol. 65, no. 24, p. 245417, Jun. 2002, doi: 10.1103/PhysRevB.65.245417.

[24] 3. %HDXFDJHDG 10RXVVHDX 1XFOHDWLRQ and crystallization process of silicon using the Stillinger-+HEHUSRWHWLDO, *Phys. Rev. B*, vol. 71, no. 9, p. 094102, Mar. 2005, doi: 10.1103/PhysRevB.71.094102.

[25] 1DJ6DWDDDG 1DLWRPLVWLFPHFKDLVPV RIRULHWDWLRQDO WHPSHUDWXUH dependence in gold-FDWDO\]HGVLOLFRQ*URZWK, *Journal of Applied Physics*, vol. 122, no. 8, p. 085106, Aug. 2017, doi: 10.1063/1.4991362.

[26] .HUUDFKH-RUEDFKDG %LGHU0ROHFXODU-dynamics computer simulation of crystal growth and melting in Al 50 1L, *EPL*, vol. 81, no. 5, p. 58001, Feb. 2008, doi: 10.1209/0295-5075/81/58001.

[27] 2EUHWH1DVKFKLHYDG 9RWDRY8LILHGGHVFULSWLRQRIWKHUDWHRIXFOHDWLR *Journal of Crystal Growth*, vol. 96, no. 4, pp. 843–848, Aug. 1989, doi: 10.1016/0022-0248(89)90644-1.

[28] D. M. Herlach, D. Simons, and P.-3LFKRUVWDOJURZWKNLHWLFVLQGHUFRROHGPHOWV of pure Ge, Si and Ge–6LDOOR\, *Philos Trans A Math Phys Eng Sci*, vol. 376, no. 2113, Feb. 2018, doi: 10.1098/rsta.2017.0205.

[29] 6.3UDGR-6LRDG (HDRWWR6XFFHVVIXOWHVWRIWKHFODVVLFDOXFOHDWLR *Computational Materials Science*, vol. 161, pp. 99–106, Apr. 2019, doi: 10.1016/j.commatsci.2019.01.023.

[30] 2.HLVWHLDG 6%UDGRQDPLFVRISDUWLDOO\IDFHWHGPHOWEURVWDOLWHUIDFHV, computational approach and single step–VRXUFHEDOFXODWLRQ, *Journal of Crystal Growth*, vol. 268, no. 1, pp. 299–319, Jul. 2004, doi: 10.1016/j.jcrysgro.2004.04.108.

[31] 0LOOHU6RPHUHPDUNVRQWKHXGHUFRROLQJRIWKH6LIDFHWDGWKH0RWHDUOR *Journal of Crystal Growth*, vol. 325, no. 1, pp. 101–103, Jun. 2011, doi: 10.1016/j.jcrysgro.2011.03.031.

[32] .DFNVR6HVSRVHWR6RPHUHPDUNVRQWKHXGHUFRROLQJRIWKH6LIDFHWDG Jackson, J. Cr VWDO*URZWK0LOOHU *Journal of Crystal Growth*, vol. 325, no. 1, p. 104, Jun. 2011, doi: 10.1016/j.jcrysgro.2011.03.040.

[33] K.-;0DGD6KLJD0RULWRDG;MLZDUDJ0LWXREVHUYDWLRQRIPXOWLSOH parallel (1 1 1) twin boundary formation from step-like grain boundary during Si

Appl. Phys. Express, vol. 13, no. 10, p. 105501, Sep. 2020, doi: 10.35848/1882-0786/abb57d.

[34] M. G. Tsoutsouva *et al.*, "Influence of grain structure and defect density on the formation and evolution during the directional solidification of 110 seeded growth silicon," *Acta Materialia*, vol. 115, pp. 210–223, Aug. 2016, doi: 10.1016/j.actamat.2016.06.004.

[35] J. Lin, M. Liu, X. Ma, and D. Yang, "Twin boundary formation at grain-boundary groove during directed growth of multicrystalline silicon ingot," *Scripta Materialia*, vol. 133, pp. 65–69, May 2017, doi: 10.1016/j.scriptamat.2017.02.028.

[36] V. Stamelou *et al.*, "Influence of grain boundary characteristics on dislocation density in directionally solidified multicrystalline silicon," *Journal of Crystal Growth*, vol. 479, pp. 1–8, Dec. 2017, doi: 10.1016/j.jcrysgro.2017.09.013.

[37] K. Kakimoto, T. Hibiya, and N. Yuge, "Effect of Grain Boundary Groove on Solidification Control of Multicrystal Silicon," *Mater. Trans.*, vol. 46, no. 5, pp. 935–943, 2005, doi: 10.2320/matertrans.46.935.

[38] T. Jasinevičius, K. Kundzinš, E. Pincuks, and G. Tamulaitis, "Twin-related and twin-free facet Si dendrites," *Acta Materialia*, vol. 53, no. 10, pp. 3021–3029, Jun. 2005, doi: 10.1016/j.actamat.2005.03.022.

[39] K. Fujiwara *et al.*, "Direct observation of the twin plane reentrant edge mechanism during the growth of polycrystalline silicon," *Acta Materialia*, vol. 56, no. 11, pp. 2663–2668, Jun. 2008, doi: 10.1016/j.actamat.2008.01.038.

[40] S. Bergmann, K. Albe, E. Flegel, D. A. Barragan-Yani, and B. Berghoff, "Modelling solid-liquid interface kinetics in silicon: an atomistically informed phase-field model," *Modelling Simul. Mater. Sci. Eng.*, vol. 25, no. 6, p. 065015, Sep. 2017, doi: 10.1088/1361-651X/aa7862.

[41] J. A. Hoerly, "Fast Monte Carlo algorithms for configurations of hard spheres," *J. Chem. Phys.*, vol. 79, no. 10, pp. 5095–5104, Nov. 1983, doi: 10.1063/1.445633.

[42] S. Plimpton, "LAMMPS Users Manual," *Sandia National Laboratory*, 2005.

[43] J. W. Lyding, G. Abeln, T.-C. Shen, C. Wang, and J. R. Tucker, "Dynamics of hydrogen in bulk silicon," *Phys. Rev. B*, vol. 31, no. 8, pp. 5262–5271, Apr. 1985, doi: 10.1103/PhysRevB.31.5262.

[44] J. J. Hoyt, M. Asta, and A. Karma, "Method for computing the anisotropy of the solid-liquid interface energy from classical molecular-dynamics fluctuations," *The Journal of Chemical Physics*, vol. 137, no. 21, p. 214108, Dec. 2012, doi: 10.1063/1.4769381.

[45] P. M. Agrawal, B. M. Rice, and D. L. Thompson, "Predicting trends in rate parameters for self-diffusion on FCC metal surfaces," *Surface Science*, vol. 515, no. 1, pp. 21–35, Aug. 2002, doi: 10.1016/S0039-6028(02)01934-5.

[46] J. Q. Broughton and G. H. Gilmer, "Molecular dynamics investigation of the crystal–fluid interface. VI. Excess surface free energies of crystal–liquid systems," *The Journal of Chemical Physics*, vol. 84, no. 10, pp. 5759–5768, May 1986, doi: 10.1063/1.449901.

[47] J. Q. Broughton and G. H. Gilmer, "Molecular dynamics investigation of the crystal–fluid interface. V. Structure of the (111) crystal–vapor interface," *The Journal of Chemical Physics*, vol. 84, no. 10, pp. 5749–5758, May 1986, doi: 10.1063/1.449900.

[48] J. Q. Broughton and G. H. Gilmer, "Molecular dynamics investigation of the crystal–fluid interface. IV. Structure of the (100) crystal–vapor interface," *The Journal of Chemical Physics*, vol. 84, no. 10, pp. 5741–5748, May 1986, doi: 10.1063/1.449899.

[49] J. Q. Broughton and G. H. Gilmer, "Molecular dynamics investigation of the crystal–fluid interface. III. Structure of the (110) crystal–vapor interface," *The Journal of Chemical Physics*, vol. 84, no. 10, pp. 5730–5740, May 1986, doi: 10.1063/1.449898.

[50] J. Q. Broughton and G. H. Gilmer, "Molecular dynamics investigation of the crystal–fluid interface. II. Structure of the (111) crystal–vapor interface," *The Journal of Chemical Physics*, vol. 84, no. 10, pp. 5717–5729, May 1986, doi: 10.1063/1.449897.

[51] J. Q. Broughton and G. H. Gilmer, "Molecular dynamics investigation of the crystal–fluid interface. I. Structure of the (100) crystal–vapor interface," *The Journal of Chemical Physics*, vol. 84, no. 10, pp. 5701–5716, May 1986, doi: 10.1063/1.449896.

[52] J. Q. Broughton and G. H. Gilmer, "Molecular dynamics investigation of the crystal–fluid interface. VII. Structure of the (110) crystal–vapor interface," *The Journal of Chemical Physics*, vol. 84, no. 10, pp. 5759–5768, May 1986, doi: 10.1063/1.449901.

[53] J. Q. Broughton and G. H. Gilmer, "Molecular dynamics investigation of the crystal–fluid interface. VI. Excess surface free energies of crystal–liquid systems," *The Journal of Chemical Physics*, vol. 84, no. 10, pp. 5759–5768, May 1986, doi: 10.1063/1.449901.

[54] J. Q. Broughton and G. H. Gilmer, "Molecular dynamics investigation of the crystal–fluid interface. V. Structure of the (111) crystal–vapor interface," *The Journal of Chemical Physics*, vol. 84, no. 10, pp. 5749–5758, May 1986, doi: 10.1063/1.449900.

Simul. Mater. Sci. Eng., vol. 18, no. 1, p. 015004, 2010, doi: 10.1088/0965-0393/18/1/015004.

[55] [illegible] in *Modern Theory of Crystal Growth I*, Berlin, Heidelberg, 1983, pp. 75–111. doi: 10.1007/978-3-642-68938-3_4.

[56] [illegible] *Canadian Journal of Physics*, Feb. 2011, doi: 10.1139/p60-044.

[57] [illegible] *Journal of Crystal Growth*, vol. 6, no. 2, pp. 205–206, Jan. 1970, doi: 10.1016/0022-0248(70)90044-8.

[58] B. Kudo, [illegible] single crystal [illegible] *Journal of Crystal Growth*, vol. 50, no. 1, pp. 247–259, Sep. 1980, doi: 10.1016/0022-0248(80)90248-1.

[59] [illegible] 4, Accessed: Mar. 26, 2021. [Online]. Available: http://adsabs.harvard.edu/abs/1984fpsa.proc..297B

[60] [illegible] *Journal of Crystal Growth*, vol. 104, no. 1, pp. 29–33, Jul. 1990, doi: 10.1016/0022-0248(90)90304-4.

[61] [illegible] *Crystals*, vol. 8, no. 1, Art. no. 1, Jan. 2018, doi: 10.3390/cryst8010036.

[62] E. P. Noronha and B. E. Ydstie, [illegible] Non-[illegible] *arXiv:2102.07747 [cond-mat, physics:nlin]*, Feb. 2021, Accessed: Jul. 07, 2021. [Online]. Available: http://arxiv.org/abs/2102.07747

635

636

637

638

639

640

641

642

643

644

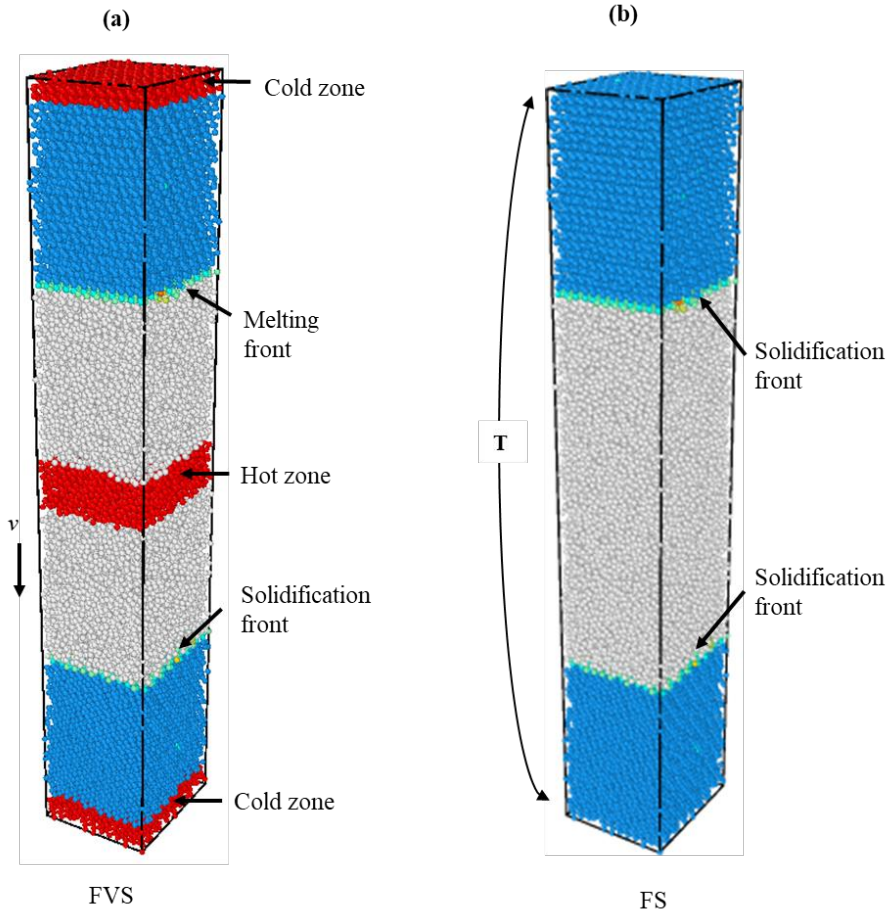

645

Figure 1: Periodic simulation domain measuring 46.33 × 53.50 × 300.69 $Å^3$ and comprising of 36,644 atoms. The blue, grey and light-green balls represent crystal, melt and interfacial atoms, respectively. (a) forced-velocity solidification (FVS) model showing the thermostatted regions colored in red (hot and cold zones kept at 2125 K and 1525 K, respectively) and direction of pulling, v (downward arrow) (b) Free-solidification (FS) model equilibrated at a uniform temperature (T) below melting point 1677 K.

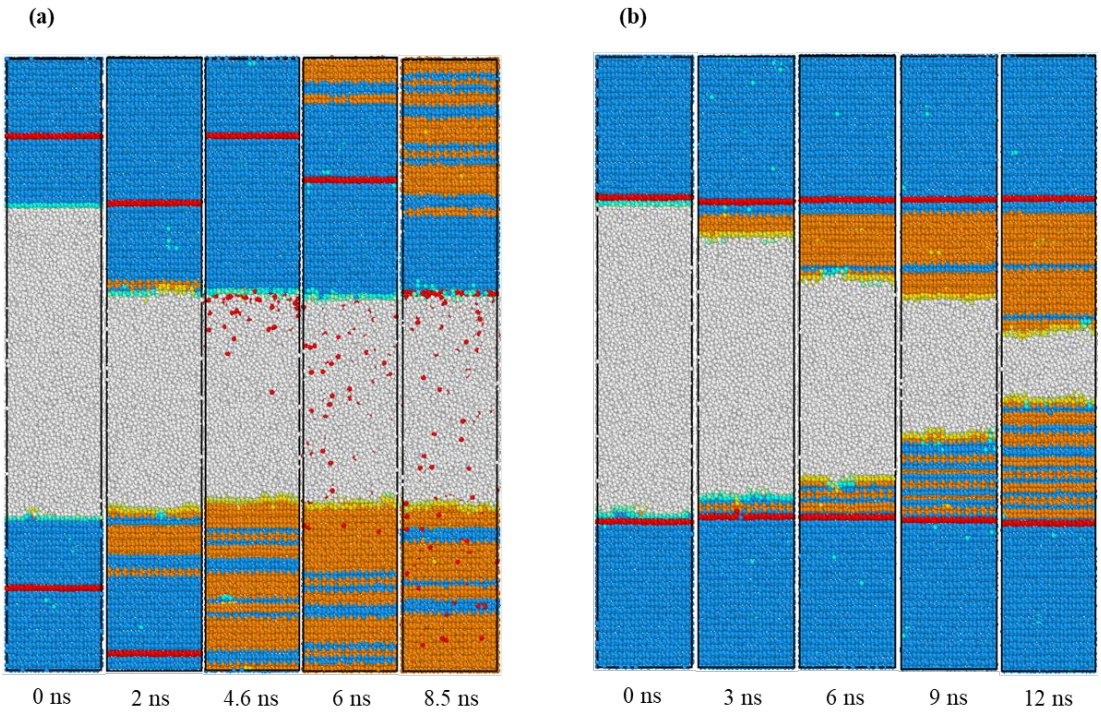

Figure 2: OVITO visualization of crystal growth in the (a) FVS model at approximately ~ 0.02 Å/ps with the red atoms showing the movement of atoms (in the crystal and liquid phases) within

reference frame during cyclic melting and solidification. Based on the extended CNA, grey balls are liquids while the blue, green, orange and yellow balls signify cubic, cubic-first neighbor, hexagonal, hexagonal-first neighbor diamond crystal structures (b) FS model at an undercooling of 24 K with red reference layers showing the symmetry between both crystal-melt interfaces

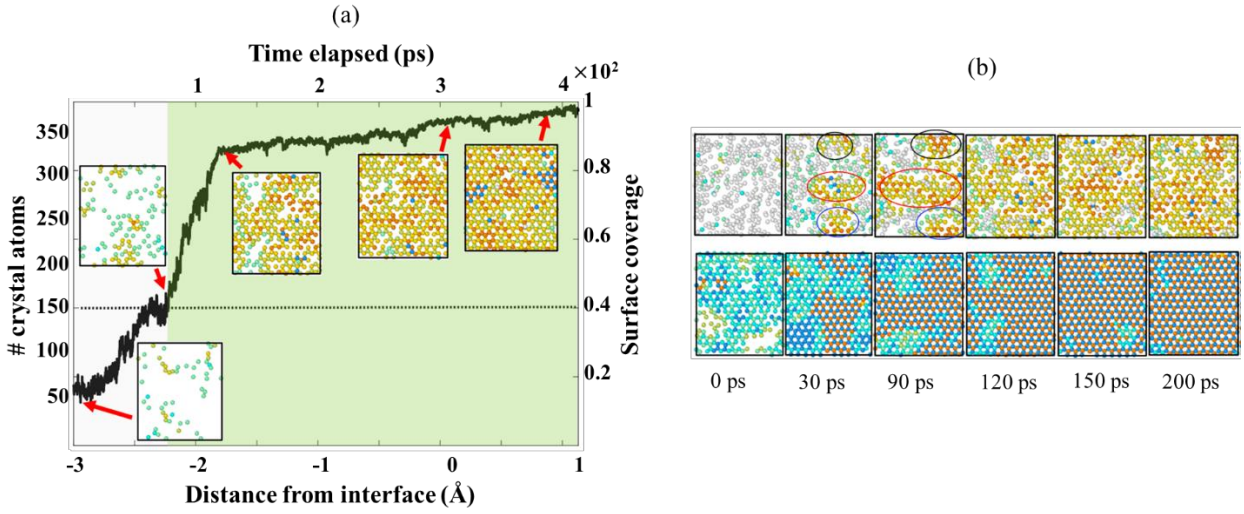

Figure 3: Evolution of a single layer from FVS model at a constant pulling of ~0.01 Å/ps (a) illustrates the nucleation-mediated growth of crystallites inside a thin slice of one atomic layer thickness as it approaches the crystal-melt interface from undercooled melt with insets showing two-dimensional expansion of Si (111) clusters (b) formation, merger and growth of smaller crystal clusters (top panels) on a completely crystal Si(111) substrate layer (bottom panels) illustrates the mechanism of layer-by-layer growth. The reference time is the point when the

substrate layer is about 90% filled with crystal atoms that had previously evolved from the melt phase.

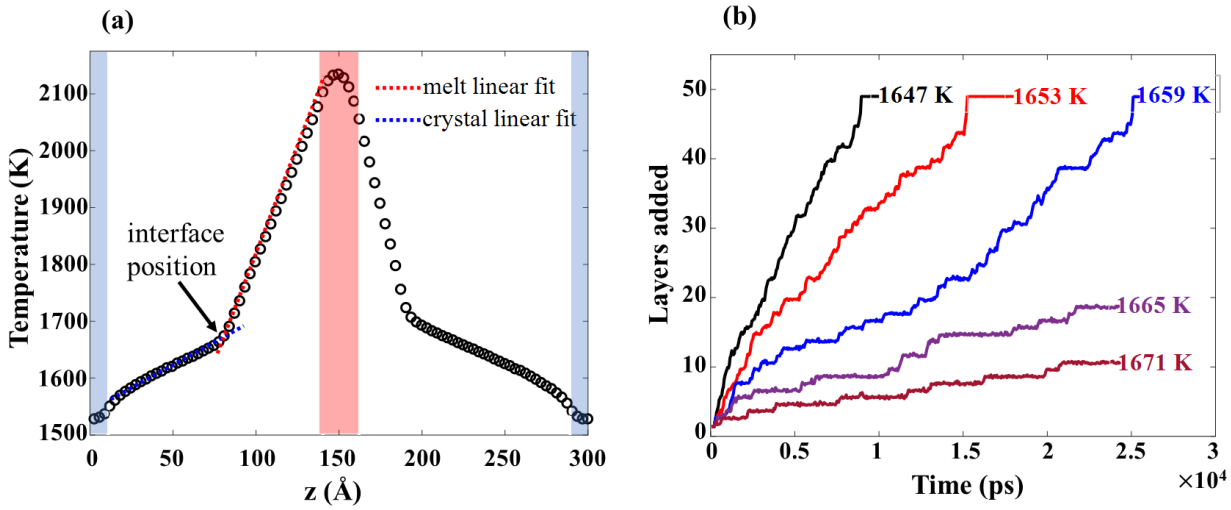

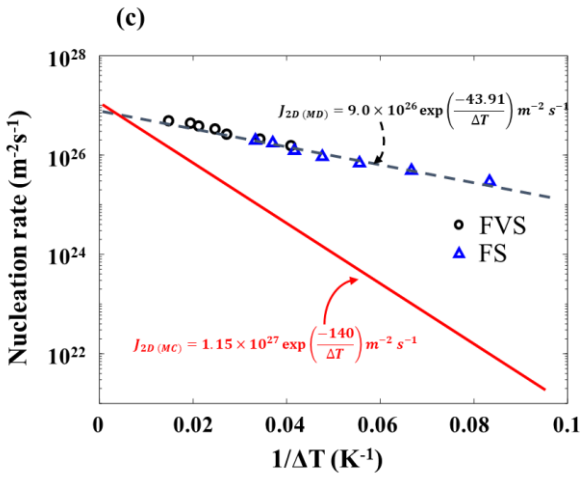

691

692 Figure 4: (a) Axial temperature profile (bin size is 3.13 Å) of FVS simulation domain at a pull
693 speed of ~0.01 Å/ps showing the determination of interface position and temperature from
694 intersection of linear fits of the solid and liquid parts of the solidification front. The light blue and
695 red column shows the positions of the cold and hot thermostats kept at 1525 K and 2125 K,
696 respectively. (b) Growth by addition of crystal layers as a function of solidification temperature in
697 the FS model. (c) Molecular dynamics nucleation rates (units in m-2s-1) as a function of the
698 reciprocal of undercooling. The black dotted line represents the nucleation rate equation fitted for
699 FVS and FS MD data. The red solid line represents nucleation rate model from Monte Carlo
700 simulations determined by ref [32].

701

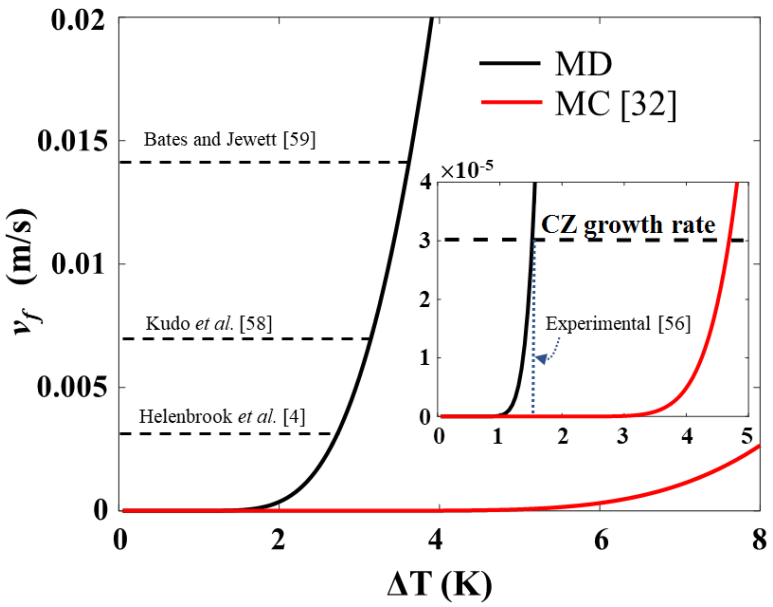

Figure 5: Si (111) facet velocity as a function of undercooling. Black curve is extrapolated from MD-derived 2D kinetic coefficient while the red curve is the prediction from MC-derived kinetic coefficient [32]. The black dotted horizontal lines represent growth rates reported from horizontal ribbon growth experiments. The inset shows the Czochralski growth rate with the blue dotted vertical line representing the experimentally reported [56] undercooling.

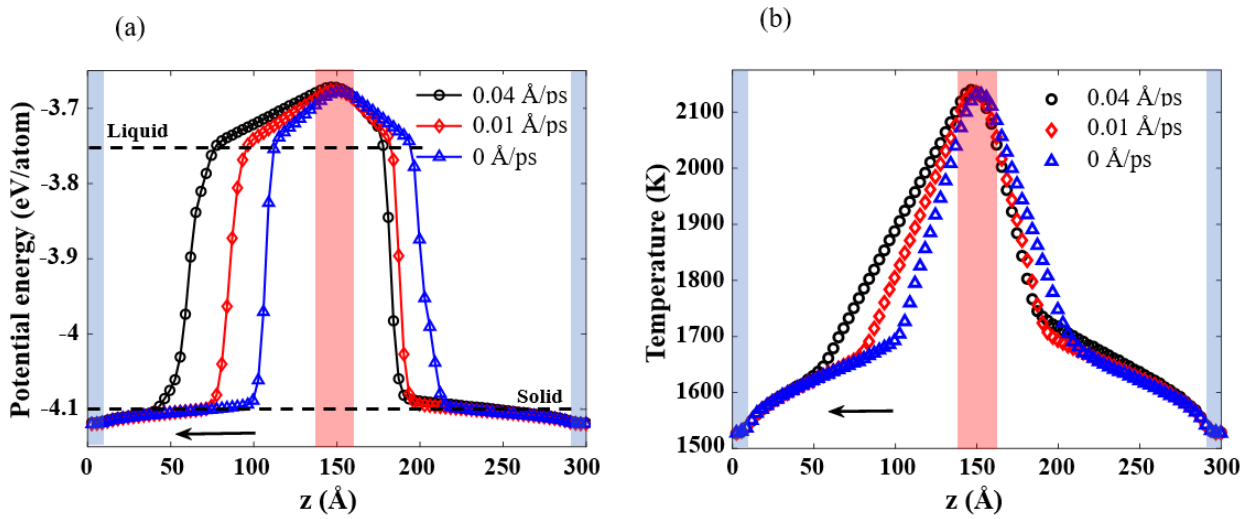

Figure 6: Description of crystal-melt interface movement and thermal profile during growth of silicon from the changes in (a) potential energy and (b) temperature profiles with increasing pull speed from the FVS model. The axial profiles are plotted using a bin size of 3.13 Å with dotted lines aiding the visualization of transition from liquid to solid energy potential, and the arrows show the direction of interface movement. The light blue and red column show the positions of the cold and hot thermostats kept at 1525 K and 2125 K, respectively.

Molecular Dynamics Study of Two-dimensional Nucleation Kinetic Coefficient for Modeling the Faceted Growth of Si (111) from an Undercooled Melt

Computational details

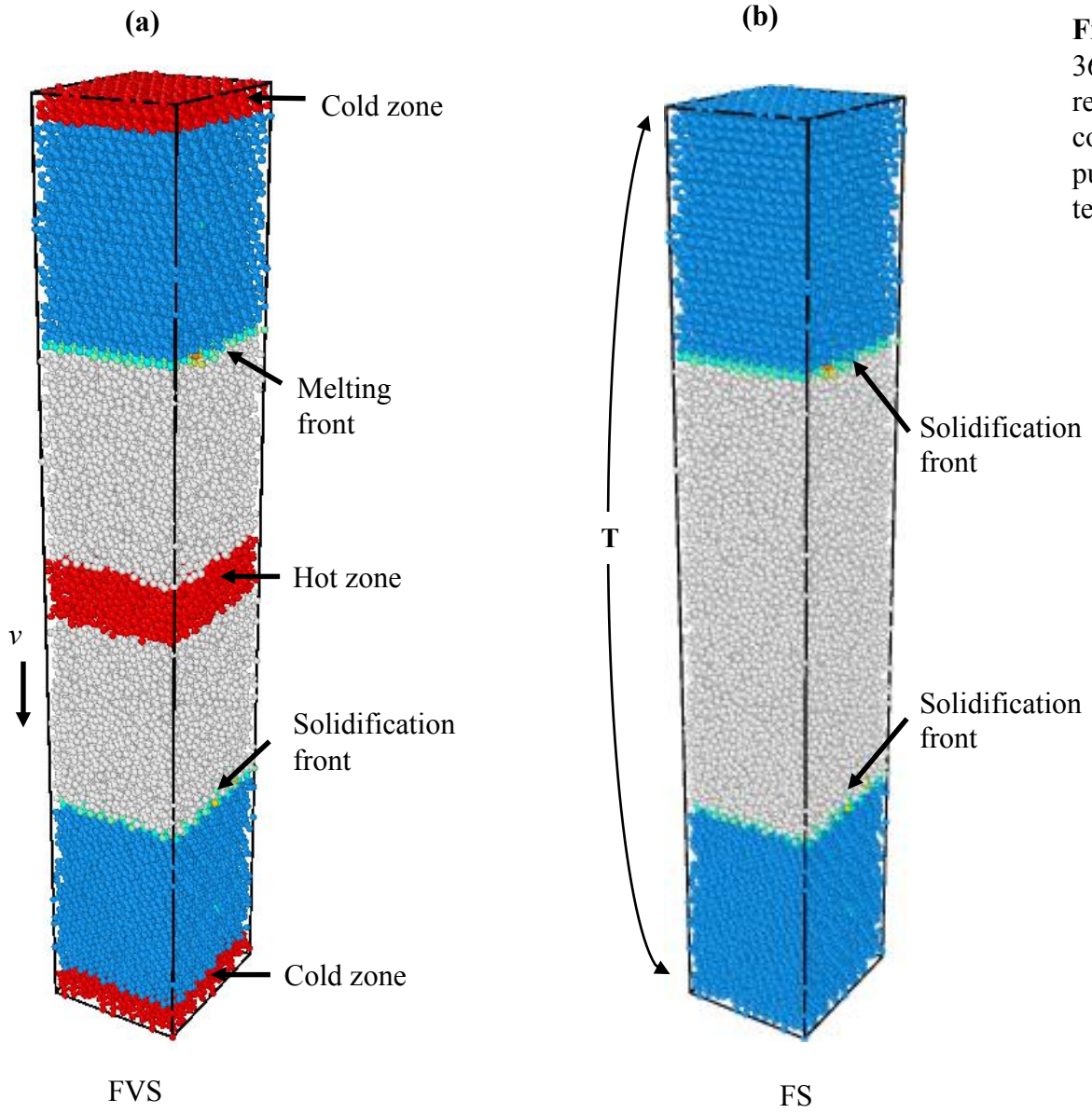

Figure 1: Periodic simulation domain measuring 46.33 ×53.50 ×300.69 Å^3 and comprising of 36,644 atoms. The blue, grey and light-green balls represent crystal, melt and interfacial atoms, respectively. (a) forced-velocity solidification (FVS) model showing the thermostatted regions colored in red (hot and cold zones kept at 2125 K and 1525 K, respectively) and direction of pulling, *v* (downward arrow) (b) Free-solidification (FS) model equilibrated at a uniform temperature (T) below melting point 1677 K.

The solidification process

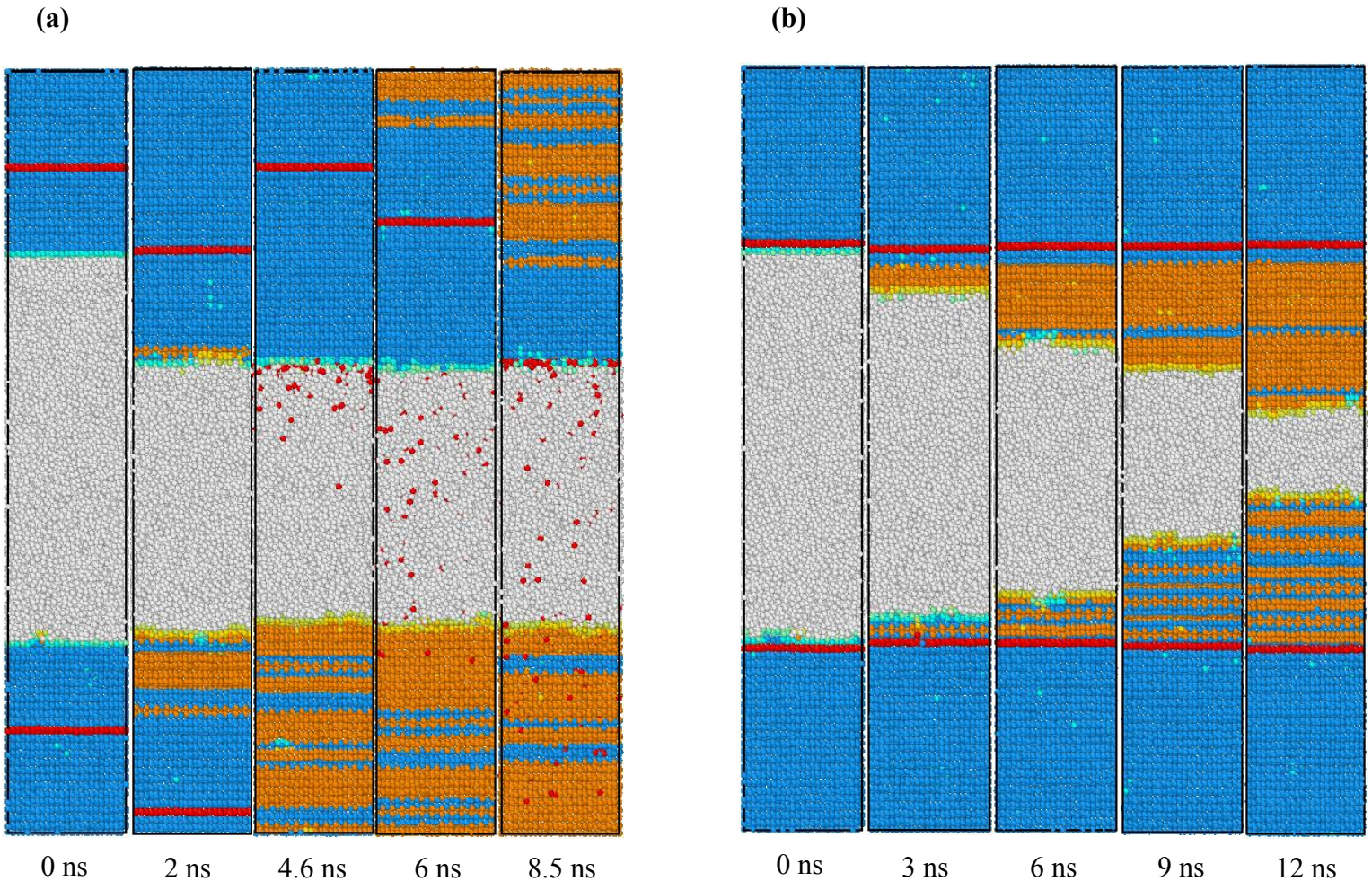

Figure 2: OVITO visualization of crystal growth in the (a) FVS model at approximately ~ 0.02 Å/ps with the red atoms showing the movement of atoms (in the crystal and liquid phases) within reference frame during cyclic melting and solidification. Based on the extended CNA, grey balls are liquids while the blue, green, orange and yellow balls signify cubic, cubic-first neighbor, hexagonal, hexagonal-first neighbor diamond crystal structures (b) FS model at an undercooling of 24 K with red reference layers showing the symmetry between both crystal-melt interfaces

Nucleation-controlled layer by layer growth from MD

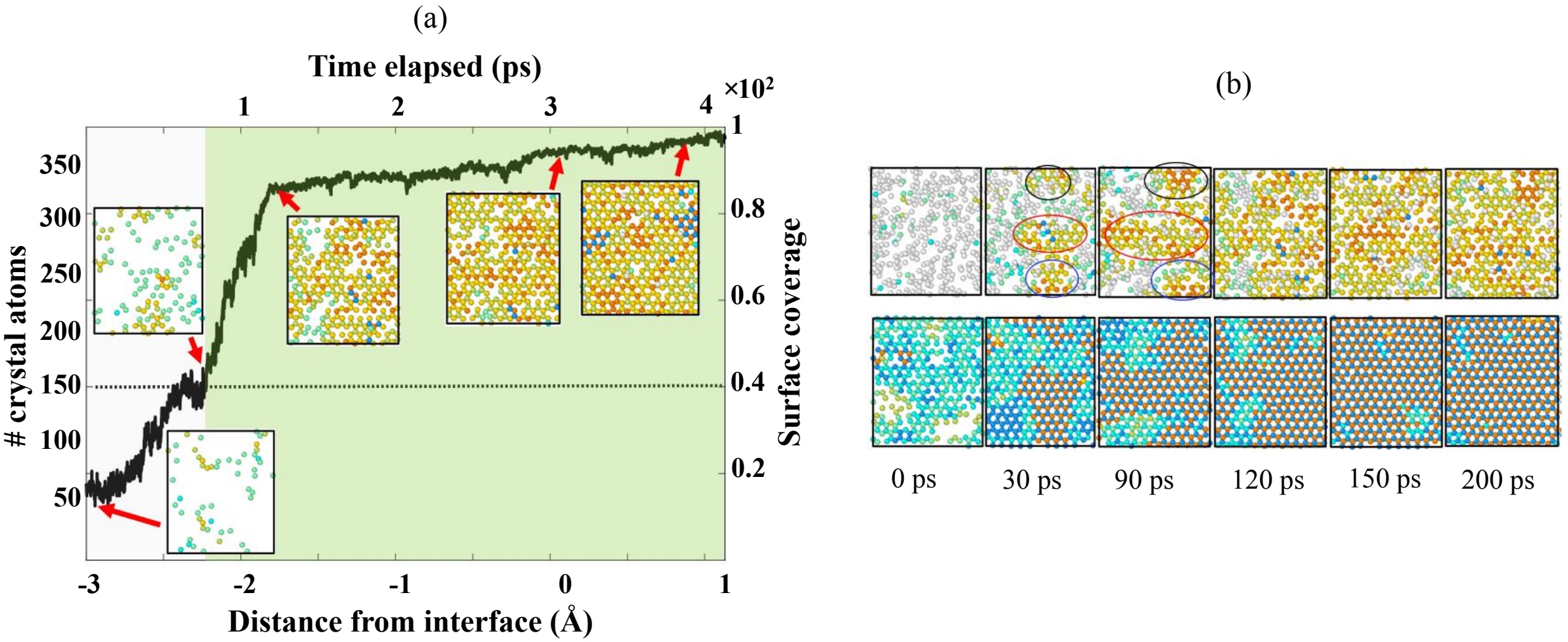

Figure 3: Evolution of a single layer from FVS model at a constant pulling of ~0.01 Å/ps (a) illustrates the nucleation-mediated growth of crystallites inside a thin slice of one atomic layer thickness as it approaches the crystal-melt interface from undercooled melt with insets showing two-dimensional expansion of Si (111) clusters (b) formation, merger and growth of smaller crystal clusters (top panels) on a completely crystal Si(111) substrate layer (bottom panels) illustrates the mechanism of layer-by-layer growth. The reference time is the point when the substrate layer is about 90% filled with crystal atoms that had previously evolved from the melt phase.

Determination of velocity and interface temperature

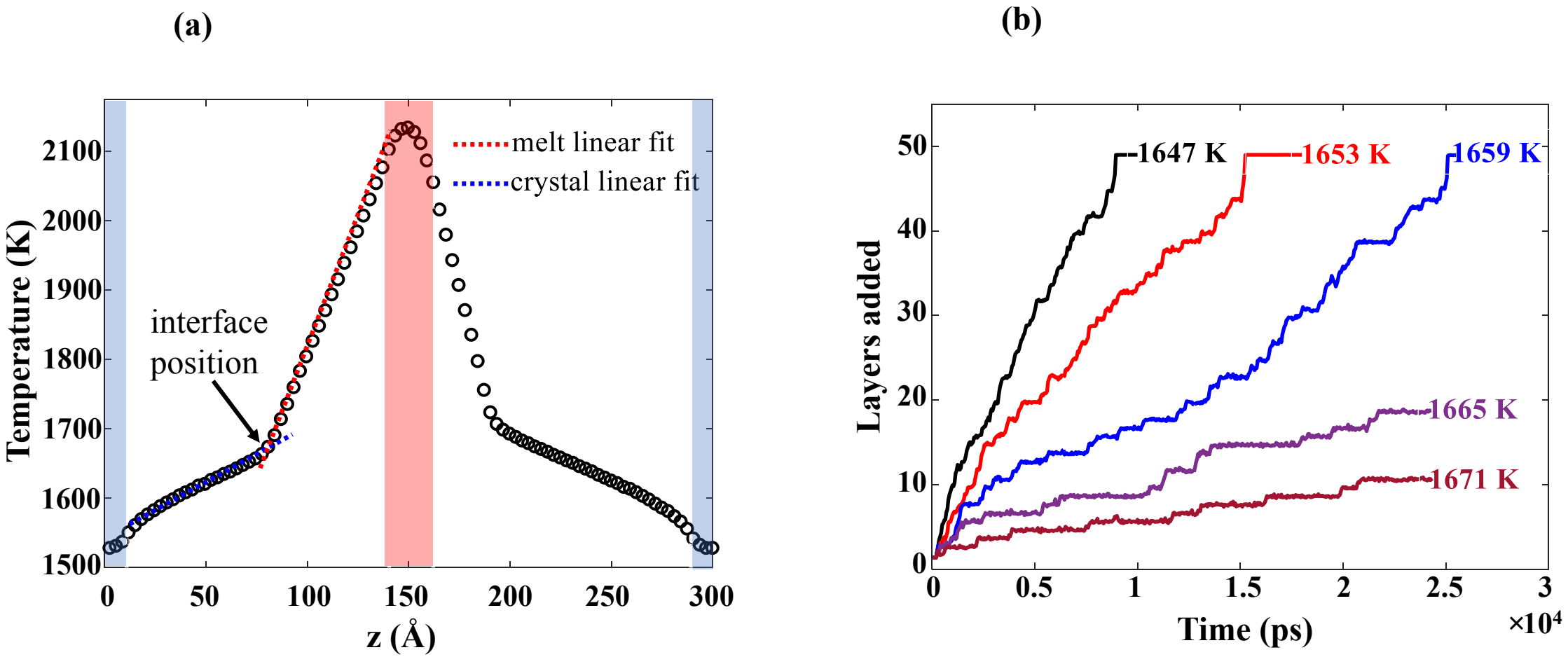

Figure 4: (a) Axial temperature profile (bin size is 3.13 Å) of FVS simulation domain at a pull speed of ~0.01 Å/ps showing the determination of interface position and temperature from intersection of linear fits of the solid and liquid parts of the solidification front. The light blue and red column shows the positions of the cold and hot thermostats kept at 1525 K and 2125 K, respectively. (b) Growth by addition of crystal layers as a function of solidification temperature in the FS model.

Nucleation rates

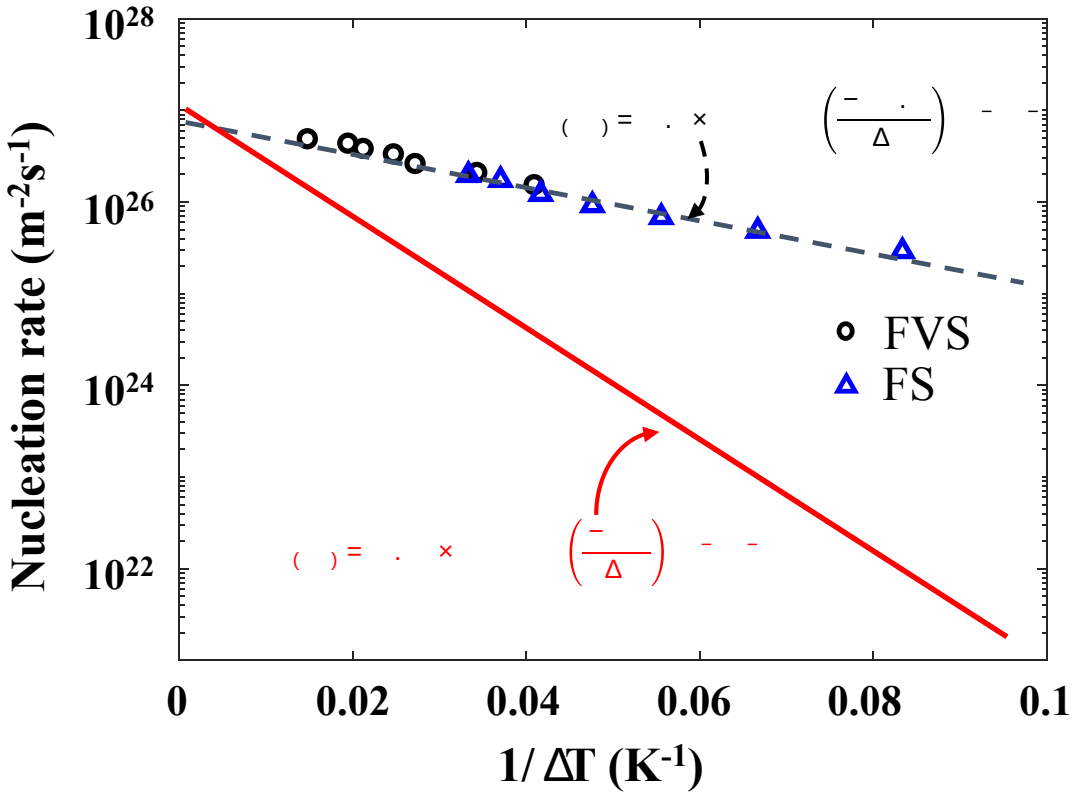

Figure 4c: Molecular dynamics nucleation rates (units in $m^{-2}s^{-1}$) as a function of the reciprocal of undercooling. The black dotted line represents the nucleation rate equation fitted for FVS and FS MD data. The red solid line represents nucleation rate model from Monte Carlo simulations determined by ref [32].

Extrapolation of MD kinetic coefficients to match real-world growth rates

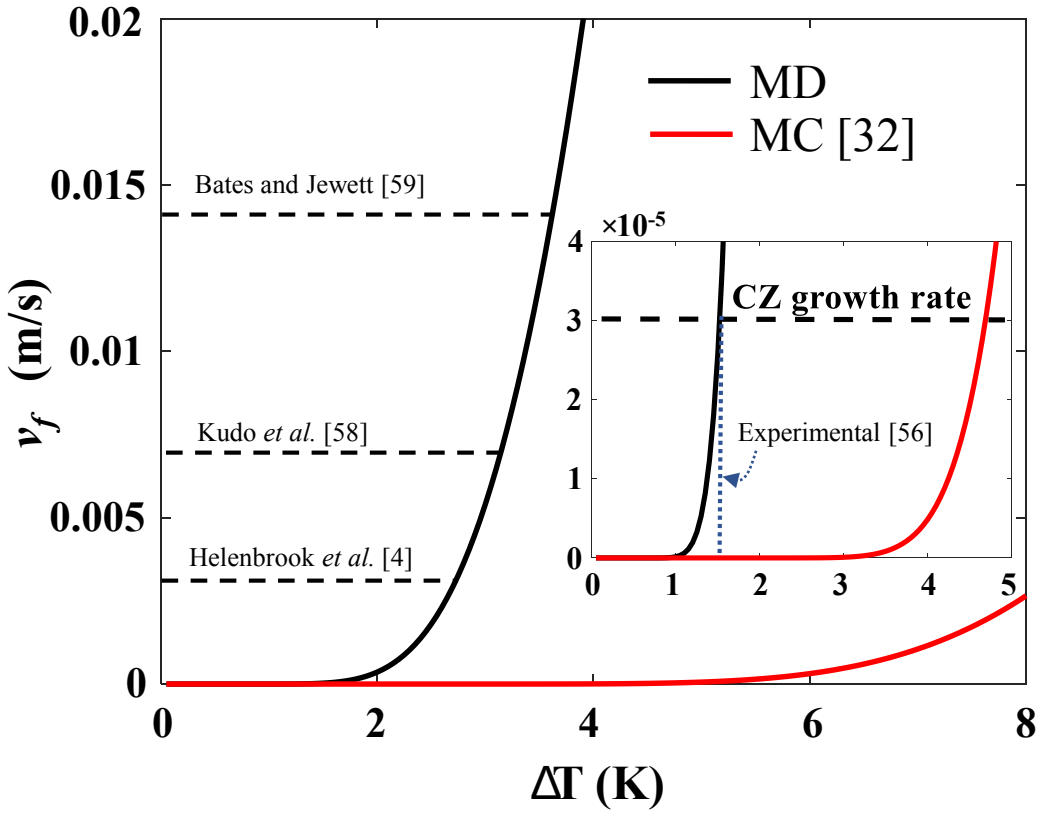

Figure 5: Si (111) facet velocity as a function of undercooling. Black curve is extrapolated from MD-derived 2D kinetic coefficient while the red curve is the prediction from MC-derived kinetic coefficient [32]. The black dotted horizontal lines represent growth rates reported from horizontal ribbon growth experiments. The inset shows the Czochralski growth rate with the blue dotted vertical line representing the experimentally reported [56] undercooling.

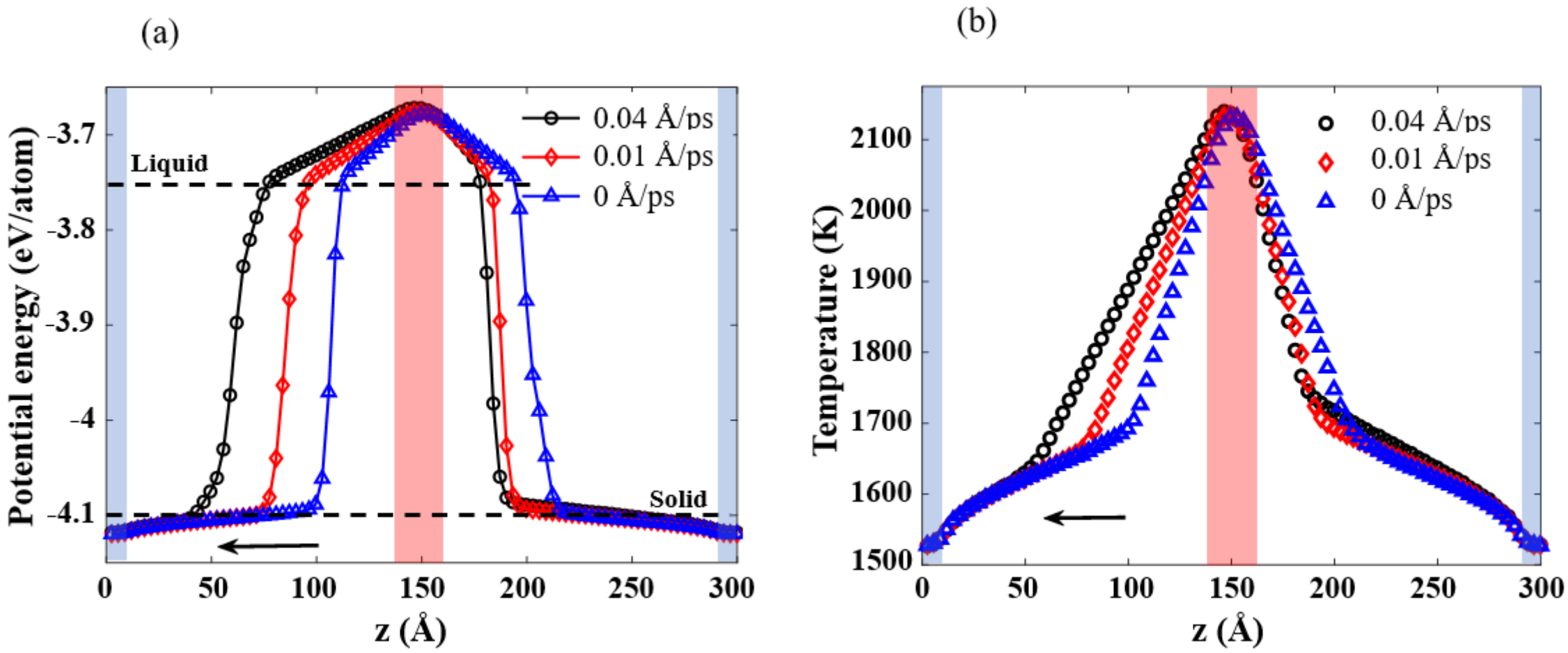

Figure 6: Description of crystal-melt interface movement and thermal profile during growth of silicon from the changes in (a) potential energy and (b) temperature profiles with increasing pull speed from the FVS model. The axial profiles are plotted using a bin size of 3.13 Å with dotted lines aiding the visualization of transition from liquid to solid energy potential, and the arrows show the direction of interface movement. The light blue and red column show the positions of the cold and hot thermostats kept at 1525 K and 2125 K, respectively.

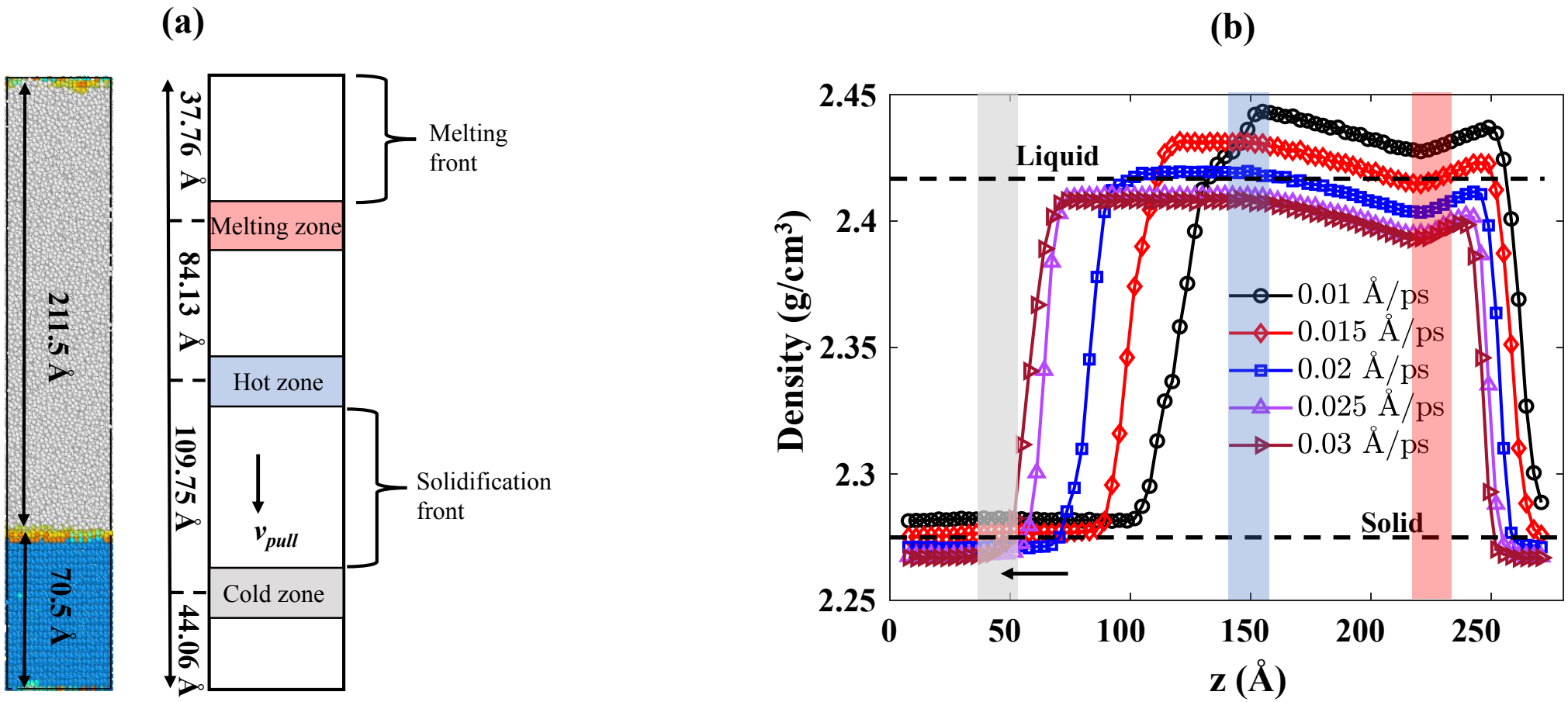

Figure S1: Summary of FVS model with a small thermal gradient of 0.36 K/Å across the solidification front and pulling (v_{pull}) applied in the downward direction. (a) The initial solid-liquid cell with larger liquid (grey atoms) region compared solid region (blue atoms) and the uneven thermal gradient across the axial direction. (b) The density profiles (bin size of 3.13 Å) with arrow showing the leftward movement of the point of transition from bulk liquid (upper dotted line) to bulk solid (lower dotted line) densities with increasing pull speed. The grey, blue and red blocks represent the positions of the cold, hot and melting zones are kept at 1670 K, 1710 K and 2000 K, respectively.

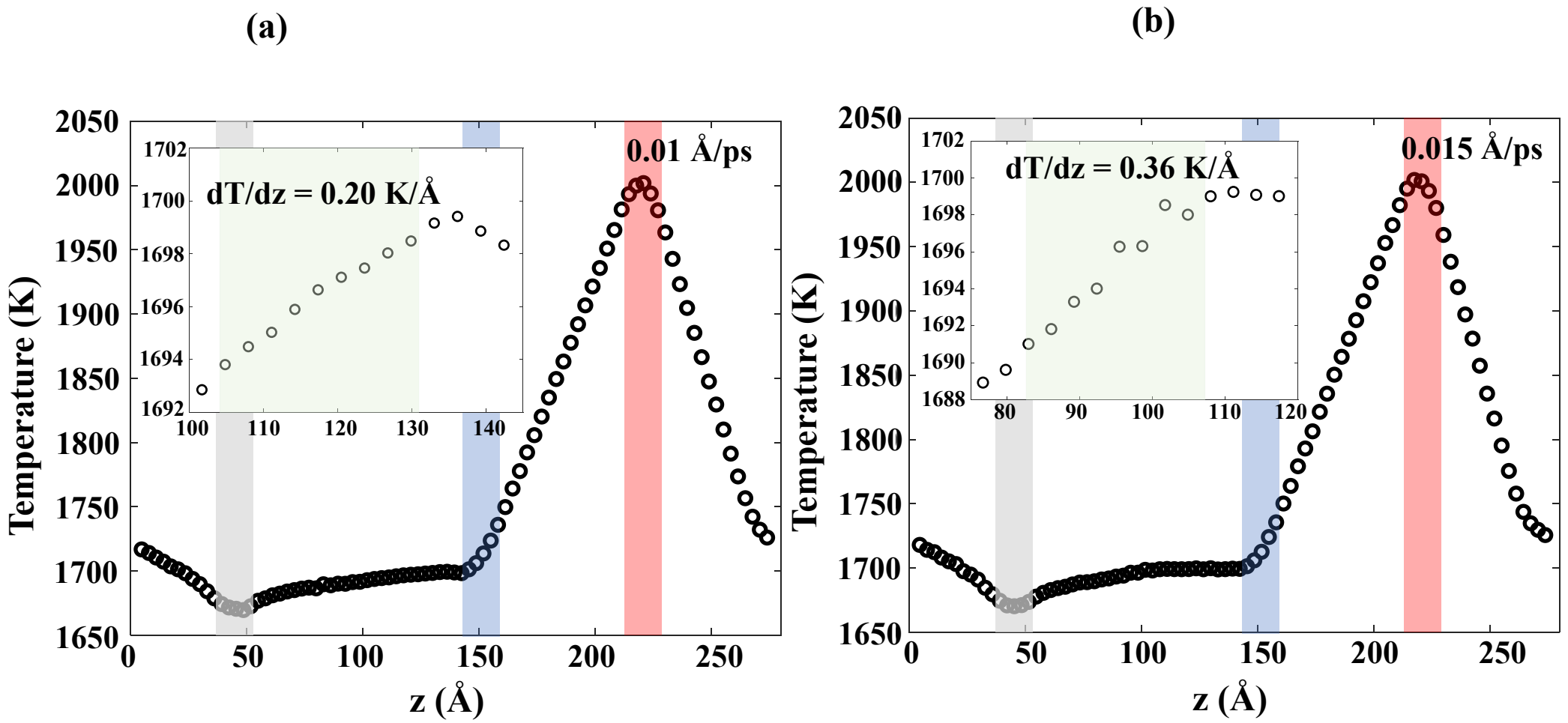

Figure S2: The axial temperature profiles (with bin size of 3.13 Å) at pulling speeds of (a) 0.01 Å/ps (b) 0.015 Å/ps (c) 0.02 Å/ps, (d) 0.025 Å/ps and (f) 0.03 Å/ps. The insets zooms in on the vicinity of the thermodynamic phase change with the region highlighted in green showing the thermal gradient across the transition region. The grey, blue and red blocks represent the positions of the cold, hot and melting zones are kept at 1670 K, 1710 K and 2000 K, respectively.

Supporting Information 2

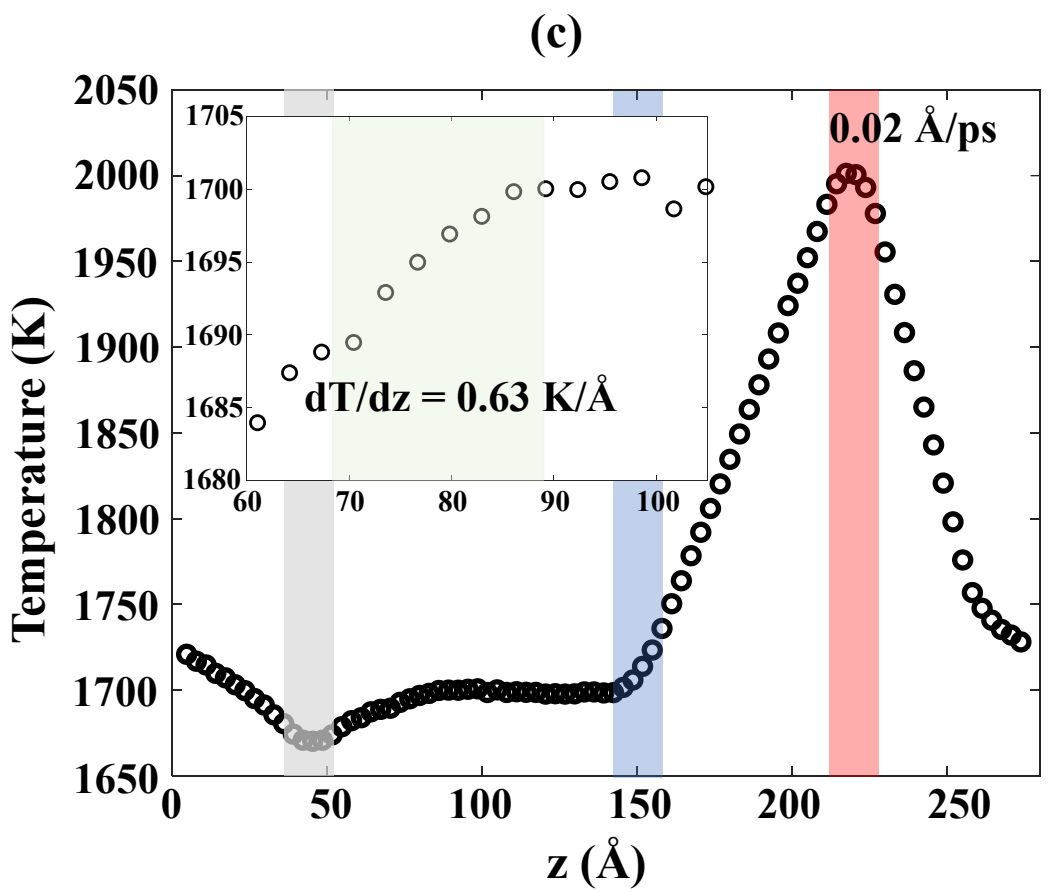

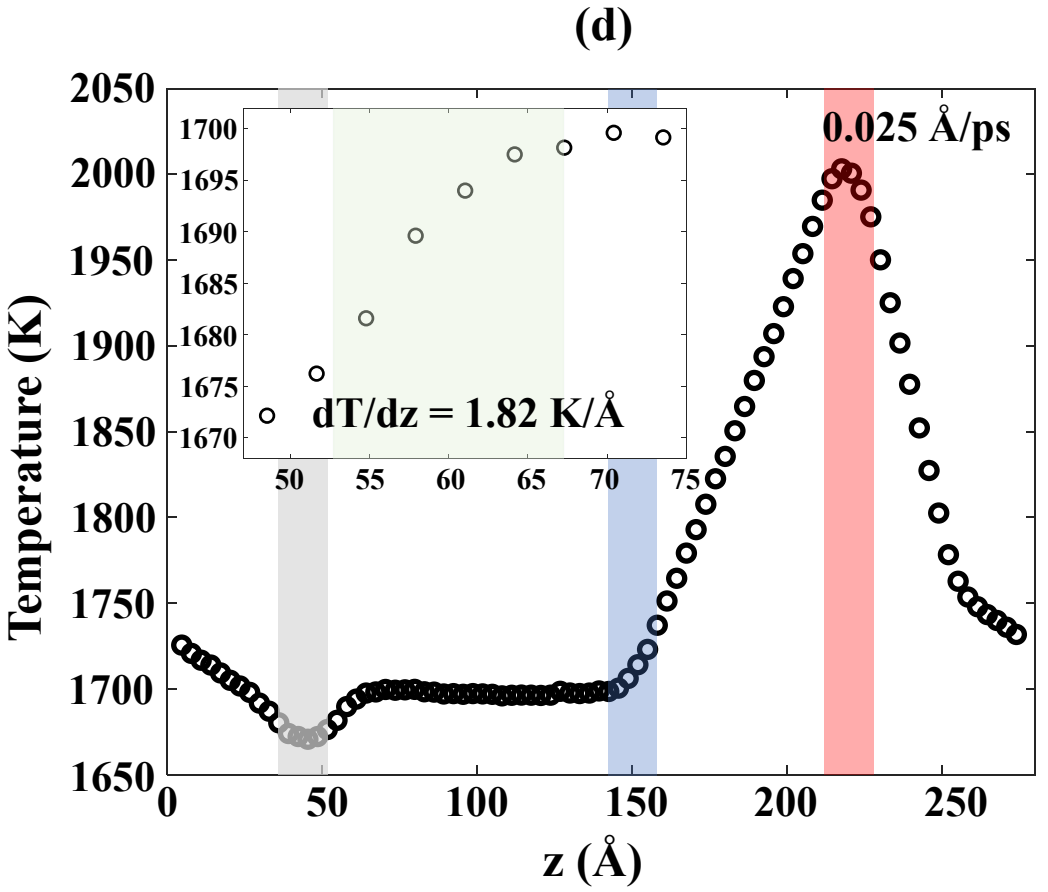

Supporting Information 2

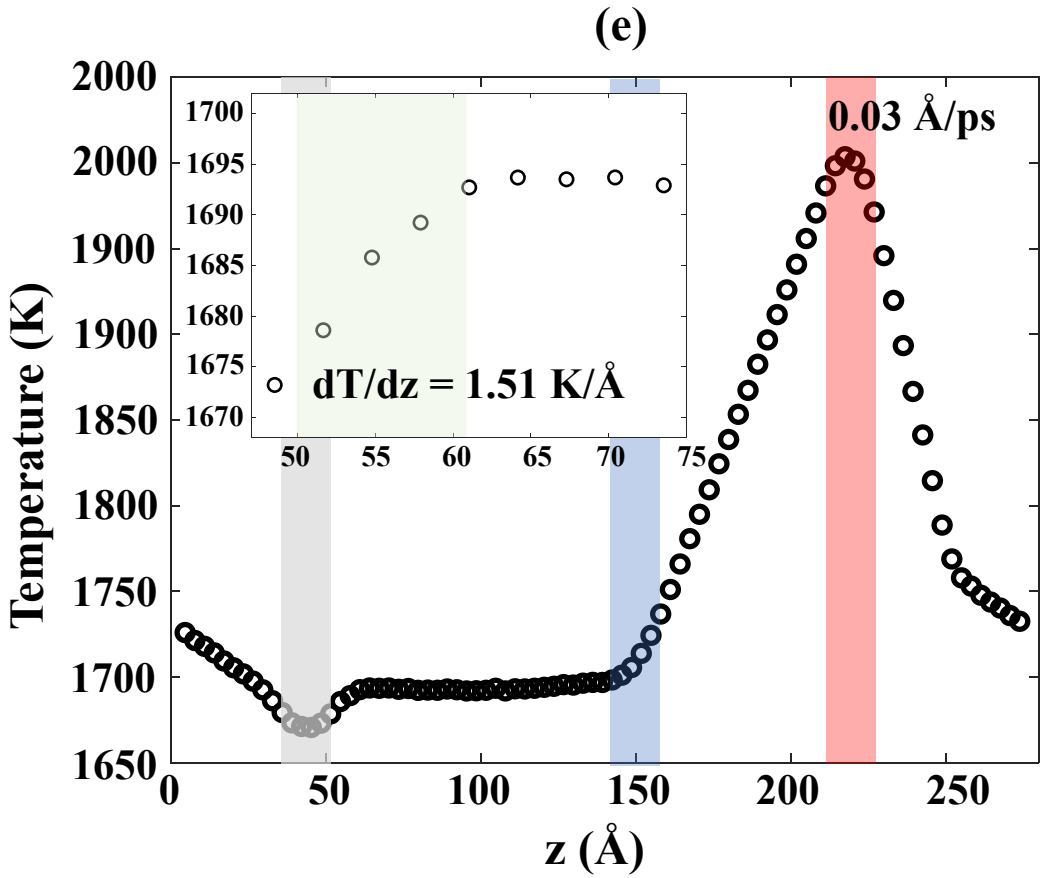

Supporting Information 3

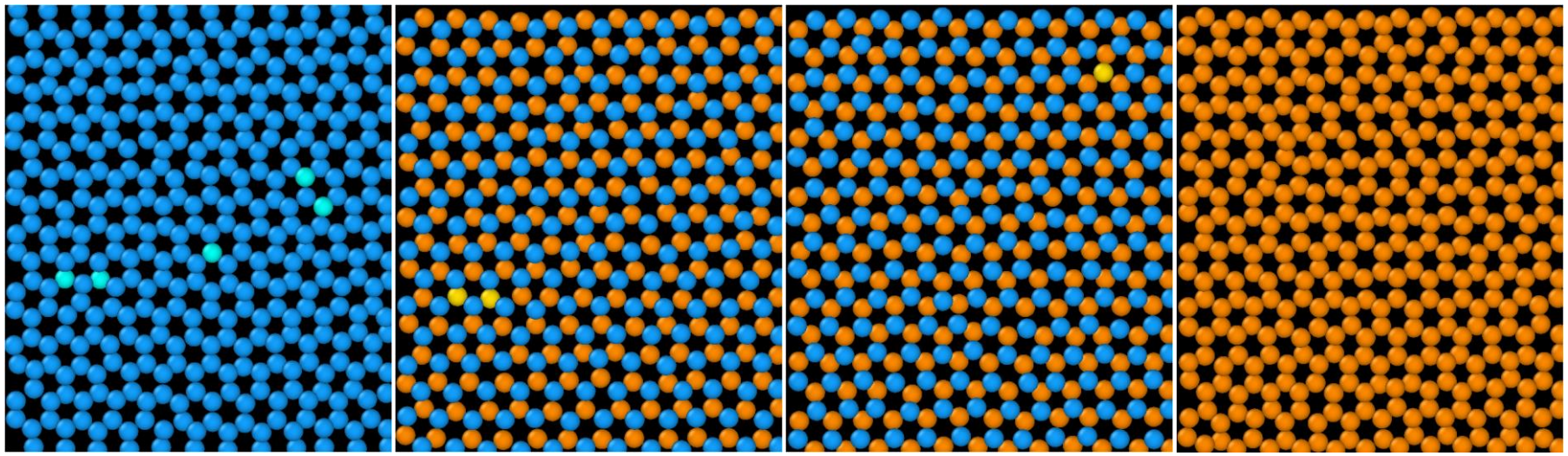

	(a)	(b)	(c)	(d)
Energy per atom	**-4.10 eV**	**-4.11 eV**	**-4.11 eV**	**-4.11 eV**
Probability (%)	**(12.4 %)**	**(21.3 %)**	**(21.3 %)**	**(45 %)**

Figure S4: Possible crystalline atomic arrangements in a Si(111) monolayer using the extended CNA implemented in OVITO. (a) cubic (b) cubic-hexagonal (c) hexagonal-cubic and (d) hexagonal diamond structures. Samples taken from simulation FVS simulations with imposed pull speed of 0.035 Å/ps.

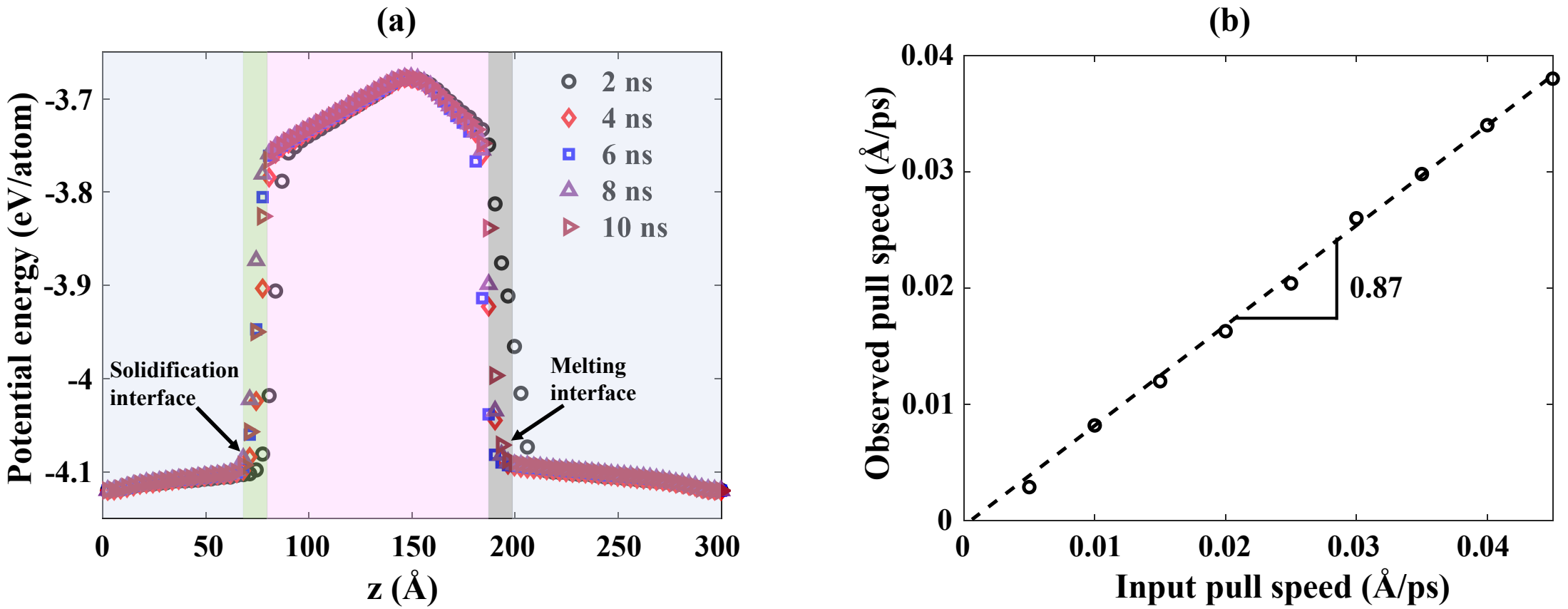

Figure S5: FVS model with 4.63 K/Å thermal gradient across the solidification and melting fronts. (a) Evolution of steady-state potential energy profile (with bin size of 3.13 Å) at pull speed of 0.02 Å/ps. (b) Comparison of input pull and observed pull speeds.

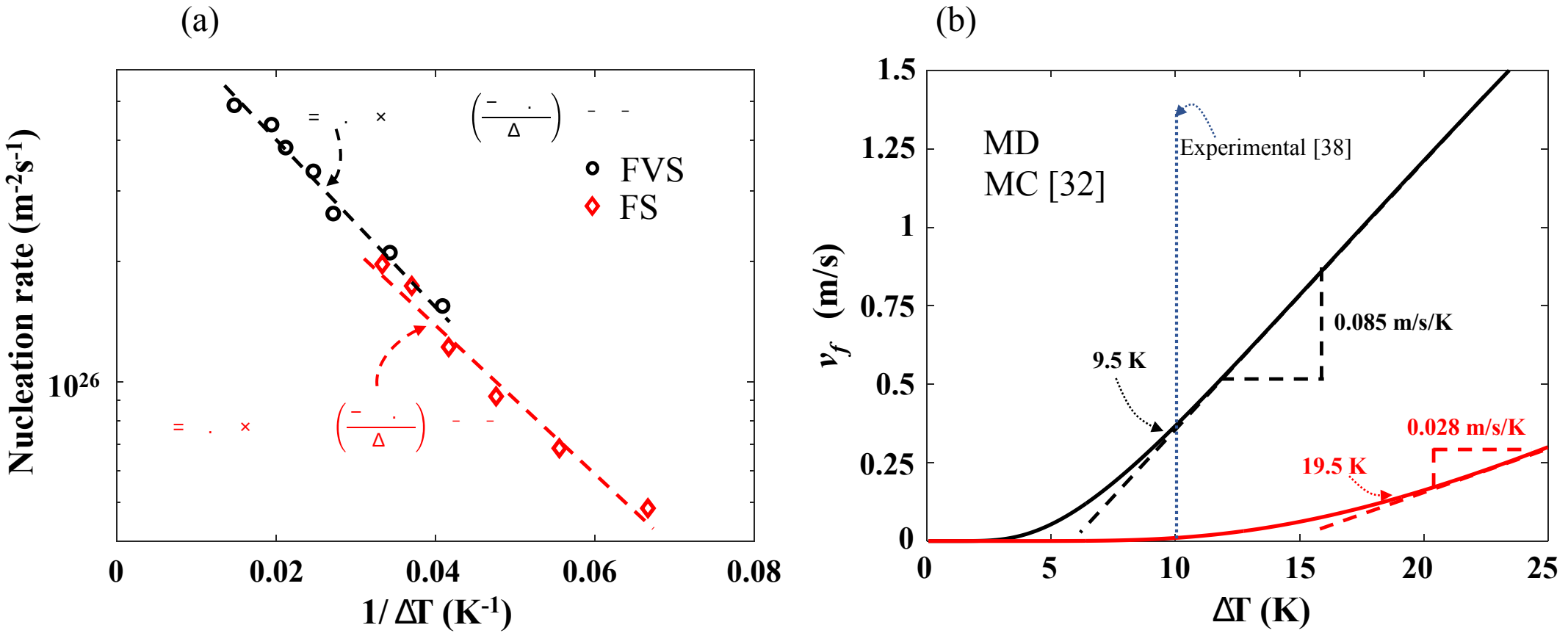

Figure S6: (a) Comparison of nucleation rates dependence on reciprocal of undercooling from the FVS and FS MD models. (b) Estimation of kinetic transition point at higher undercooling for MD and MC [32] kinetic models from the slopes of linear regime of their respective facet velocity versus undercooling curve. The black and red dotted lines represent the linear fits from MD and MC curves, respectively, and the blue dotted vertical line represents the onset of faceted-dendrite growth determined from experimental observation [38].